Journal of African Earth Sciences 222 (2025) 105475

Contents lists available at ScienceDirect

Journal of African Earth Sciences

journal homepage: www.elsevier.com/locate/jafrearsci

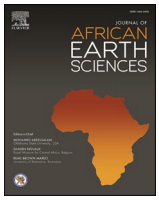

Petrology and geochemistry of the Suhum Basin granitoid complex, Ghana: Implications for crustal growth during the Rhyacian orogeny of the West African Craton

Daniel Kwayisi [a,b], Prince Ofori Amponsah [a,*], Emmanuel Kwaku Awunyo [c], Marian Selorm Sapah [a], Patrick Asamoah Sakyi [a,d], Ben-Xun Su [d], Prosper M. Nude [a], Abigail Enyonam Ayikwei [a], Eric Dominic Forson [e]

[a] Department of Earth Science, School of Physical and Mathematical Sciences, University of Ghana, P. O. Box LG58, Legon-Accra, Ghana
[b] Department of Earth Science, University of Johannesburg, Auckland Park Kingsway Campus, South Africa
[c] Minerals Commission, #12 Switchback Road Residential Area, Cantonment-Accra, Ghana
[d] Key Laboratory of Mineral Resources, Institute of Geology and Geophysics, Chinese Academy of Sciences, Beijing, 100029, China
[e] Department of Physics, School of Physical and Mathematical Sciences, University of Ghana, Legon-Accra, Ghana

ARTICLE INFO

Handling Editor: DR Damien Delvaux

Keywords:
Paleoproterozoic
Birimian
Granite Gneiss
Migmatite
West African Craton
Suhum Basin

ABSTRACT

The Suhum Basin granitoid complex is an important granitoid complex of the Birimian terrane of Ghana for unravelling the crustal growth and evolution of the West African Craton (WAC) during the Rhyacian Eburnean orogeny. Almost the entire Suhum Basin is occupied by an extensive granitoid complex, which contains useful information for constraining debatable plate tectonic issues, especially during the Archean-Paleoproterozoic transition period. We present petrography, whole-rock geochemistry, and mineral chemistry data of biotite, amphibole, and plagioclase to constrain the temperature-pressure conditions of emplacement, petrogenesis, tectonic setting, the evolution of the granitoids complex of the Suhum Basin, and its implications for the crustal growth and evolution of the WAC. Four lithological types; granite gneiss, migmatites, leucogranites, and mafic enclaves, characterise the granitoid complex of the Suhum Basin. Biotites from the granitoid complex have an annite-siderophyllite composition, and that, coupled with their calc-alkaline and I-type signatures, indicates crystallisation of the granitoid complex of the Suhum Basin under oxidised conditions. The medium-to high-K character of the rocks, together with the calc-alkaline nature, may be a reflection of the generation of magma in regions where the mantle wedge might have interacted with enriched fluids from the underlying plate during dehydration. The enrichment of LILE and LREE relative to HREE and HFSE and the negative Eu, Nb-Ta, and Ti anomalies of the granitoids complex may indicate derivation from enriched magma sources with varying degrees of fractionation in an arc environment. Amphibole-plagioclase thermobarometry indicates that the granitoid complex formed at P-T conditions of 600–712 °C and 5.2–7.2 kbar, signifying a deeper depth (19–27 km) of emplacement. The overall geochemical data suggest that the rocks formed during a single orogenic event related to a volcanic arc environment where subduction zone components played a role in the generation of their parental magmas. This finding is therefore consistent with the onset of "modern-style" subduction-related processes during the Archean-Paleoproterozoic transitional period.

1. Introduction

Studies of granitoids have advanced our understanding of crustal growth and evolution in the history of the continental crust (e.g., Rudnick and Fountain, 1995; Barbarin, 1999; Rudnick and Gao, 2003; Hawkesworth et al., 2010; Spencer et al., 2017). This is because the mineralogical and geochemical compositions of granitoids provide very useful information that has been used to constrain debatable plate tectonic issues, especially during the Archean-Paleoproterozoic transition period (Gong et al., 2019). Integrated studies involving petrography, major and trace elements, and mineral chemistry of amphibole and biotite can provide important constraints on the magmatic evolution,

* Corresponding author.
E-mail address: pamponsah@ug.edu.gh (P.O. Amponsah).

https://doi.org/10.1016/j.jafrearsci.2024.105475
Received 20 March 2024; Received in revised form 18 October 2024; Accepted 5 November 2024
Available online 12 November 2024
1464-343X/

P-T condition of crystallisation, oxidation state of magma, depth and emplacement, petrogenesis, and geodynamic setting of granitoids (Abdel-Rahman, 1994; Shabani et al., 2003; Uchida et al., 2007; Sakyi et al., 2020a). Thus, it is crucial to study granitoids to understand our dynamic planet.

The Paleoproterozoic Birimian terrane of the Leo-Man shield forms an integral segment of the West African Craton (WAC) that has received considerable attention in research studies due to its immense wealth in both precious and base metals (Lompo, 2009; Sakyi et al., 2014; Diatta et al., 2017; Grenholm et al., 2019). The Birimian terrane comprises a series of greenstone belts and metasedimentary basins intruded by several generations of granitoids formed during Eburnean tectono-magmatic and metamorphic events (e.g., Hirdes et al., 1992; Gasquet et al., 2003; Baratoux et al., 2011; de Kock et al., 2011; Sakyi et al., 2014; Anum et al., 2015; Grenholm et al., 2019; Forson et al., 2021; Masurel et al., 2022; Amponsah and Forson, 2024). This age falls outside the main peaks of global magmatic activity: ca. 3.8–3.5 Ga; 2.9–2.6 Ga; 1.9–1.6 Ga; 1.2–0.9 Ga; 0.6–0 Ga (e.g., Gastil, 1960; Abouchami et al.,

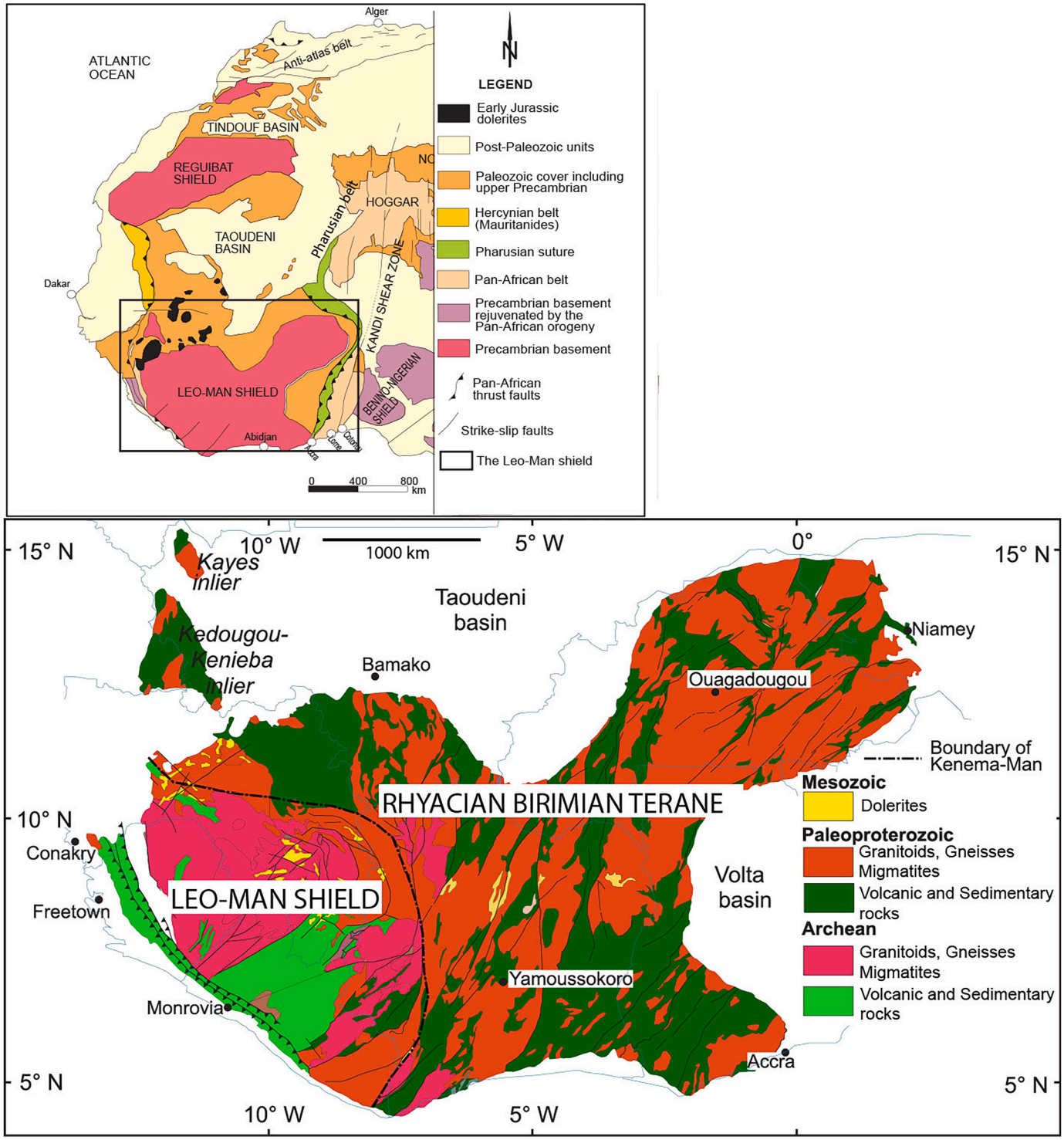

Fig. 1. Simplified geological map of the Leo-Man Shield of the West African Craton, clearly illustrating regions where the Paleoproterozoic Birimian crust is exposed (modified after Milési et al., 1992).

1990; Condie, 1998; Condie et al., 2009). The Birimian terrane thus presents an avenue to properly constrain the rates of early crustal growth, accretion, and stabilization mechanisms during the transitional Archean-Proterozoic period.

The Birimian terrane in Ghana comprises six major greenstone belts with five intervening metasedimentary basins and is intruded by several suites of basin- and belt-type granitoids (Hirdes et al., 1992; Forson and Amponsah, 2023; Forson et al., 2024). The Suhum Basin is an important basin of the Birimian terrane of Ghana for unravelling the crustal growth and evolution of the WAC during the Rhyacian Eburnean orogeny. This is because, unlike the other basins, almost the entire Suhum Basin is occupied by an extensive granitoid, gneisses and migmatite complexes, which are partly granitic gneisses and migmatites of varying ages (Agyei Duodu et al., 2009). Although, some studies have been conducted in the Suhum Basin, only a few dealt with petrogenetic evolution, pressure-temperature and depth estimations and their implications for crustal growth and evolution of the WAC using mineral chemistry and whole-rock geochemical data (e.g., Opare-Addo et al., 1993; John et al., 1999; Klemd et al., 2002; Galipp et al., 2003; White et al., 2013). Recent studies on the granitoids complex of the Suhum Basin have suggested the evolution from Paleoproterozoic juvenile mantle component and recycled Neoarchean materials (Amponsah et al., 2023). Nonetheless, detailed studies of petrography, geochemistry, and mineral chemistry to investigate the petrogenetic evolution, P-T conditions of crystallisation, and depth and geodynamic setting of emplacement of the granitoid complex are generally lacking. These granitoids, however, are composed of biotite and amphibole, which are important tectonomagmatic indicators in the study of the petrogenesis of granitoids (Abdel-Rahman, 1994; Shabani et al., 2003). Hence, the main aim of this paper is to expound the geological conditions for the formation of these granitoids, of the Suhum Basin, which will in turn aid in constraining the crustal growth and evolution of the WAC, by integrating their petrography, mineral chemistry, and whole-rock major and trace element compositions. Thus, the geothermobarometric conditions, depth of emplacement and the nature of the magma during the emplacement of these rocks will be determined. In addition, the petrogenesis and tectonic settings will be evaluated using the mineral chemical data of biotite, amphibole, and plagioclase, whole-rock geochemical data and petrographic studies.

2. Geological setting

2.1. The Leo-Man Shield

The southern part of the West Africa Craton (sWAC), known as the Leo-Man Shield, is composed of eastern and western geological domains that straddle countries such as Ivory Coast, Burkina Faso, Mali, Liberia, Sierra Leone, Senegal, Niger, and the western half of Ghana (Fig. 1). The western domain also referred to as the Archean Kenema-Man domain, consists of metamorphic rocks, granitoids and metamorphosed supracrustal greenstone belts whereas the eastern Paleoproterozoic domain or the Baoule-Mossi domain (i.e. the Birimian terrane), is composed of volcano-sedimentary (greenstone) belts and terrigenous (metasedimentary) basins intruded by syn-to late-Eburnean granitoids (Fig. 1; Bonhomme, 1962; Leube et al., 1990; Feybesse et al., 2006; Thiéblemont et al., 2004, Salvi et al., 2016; Sapah et al., 2021; Nunoo et al., 2022a; Adams et al., 2023; Forson et al., 2023; Forson and Amponsah, 2023; Forson et al., 2024). The Archean and Paleoproterozoic domains have been affected by three main tectonomagmatic and metamorphic events. These are the Leonian events at ~3200–3000 Ma, Liberian events at ~2900–2700 Ma, and Eburnean orogeny at ~2250–2060 Ma (e.g., Baratoux et al., 2011; Tshibubudze et al., 2013; Sakyi et al., 2014; Anum et al., 2015; Kouamelan et al., 2015; Block et al., 2016a).

2.2. Overview of the Birimian terrane in Ghana

The Birimian terrane in Ghana is characterised by successions of sub-parallel, generally NE-SW trending greenstone belts separated at somewhat regular intervals by metasedimentary basins. From southeast to northwest these are the Suhum Basin, Kibi-Winneba belt, Cape Coast Basin, Ashanti belt, Kumasi Basin, Sefwi belt, Sunyani Basin, Bui belt, Maluwe Basin, and Bole-Nangodi belt) (Fig. 2a; Leube et al., 1990; Sylvester and Attoh, 1992; Jessell et al., 2012; Senyah et al., 2016; Feng et al., 2018; Asiedu et al., 2019; Sakyi et al., 2014, 2020a, 2020b; Nunoo et al., 2022b; Amponsah and Forson, 2023; Amponsah and Forson, 2024). Feybesse et al. (2006) proposed a coeval deposition between the rocks of the Birimian greenstone belts and metasedimentary basins. The belts are 15–40 km wide and 60–90 km apart and decrease in width north-westward across the country (Taylor et al., 1992; Nunoo et al., 2016; Feng et al., 2019). However, the Lawra belt located in northwestern Ghana trends N-S and constitutes the southern extension of the larger Boromo greenstone belt, exposed in southern Burkina Faso (Amponsah et al., 2016a and b; Block et al., 2016b).

The volcanic greenstone belts predominately comprise tholeiitic basalts and basaltic andesite superimposed by calc-alkaline dacites and andesites interbedded with volcaniclastic sediments (Leube et al., 1990; Sylvester and Attoh, 1992; Kazapoe et al., 2022; Agra et al., 2023). Minor mafic intrusions crosscut the volcanics, with small ultramafic bodies occurring locally in some places. The metasedimentary basins of the Birimian terrane are composed mainly of metasedimentary rocks, including metagreywacke, phyllites, metacherts, and metaargillite (Sakyi et al., 2018; 2019; Atanga et al., 2023; Kazapoe et al., 2023).

Four main generations of granitoid suites, namely Cape Coast, Winneba, Bongo, and Dixcove type granitoids, intrude these volcano-sedimentary belts and basins (Fig. 2a). The Winneba type is granodioritic to granitic in composition and limited to a small area close to Winneba in south-eastern Ghana; the Cape Coast type is largely biotite-granodiorites with peraluminous characteristics; the Dixcove type, which predominantly intrudes the volcanic belts, is usually hornblende-bearing granitoid types with metaluminous affinities; while the younger Bongo type granitoids are K-rich granitoids located mainly in the volcanic belts in northern Ghana, and also intrude the Tarkawaian sequences (Leube et al., 1990; Anum et al., 2015; Abitty et al., 2016; Sakyi et al., 2020a).

2.3. Geology of the suhum basin

The ~3,277 km^2 NE-SW trending lobate-shaped Suhum Basin is located in southern Ghana and boarded to the NE by the Voltaian supergroup, to the SE by the Pan-African mobile belt and to the west by the Cape-Coast basin and the Kibi-Winneba greenstone belt (Fig. 2a and b). The Suhum Basin is underlain almost entirely of granitoid complex and sediments at the fringes (Agyei-Duodu et al., 2009). These complexes are composed of various granitoid intrusions with migmatitic and gneissic components. The granitoid complex in the Suhum Basin can be divided into four main types (Fig. 2b). The type 1 granitoid complex was emplaced between 2187 ± 1 Ma (U-Pb zircon dating by Loh et al. (1999)) and 2165 ± 9 Ma (U-Pb zircon dating by Opare-Addo et al. (1993)) and composed of biotite (± hornblende ± muscovite) gneiss with local migmatitic and minor biotite schists. Type 2 granitoid, which is the most extensive in the Suhum basin and termed the "Tamnean protolith" by Agyei-Duodu et al. (2009), was emplaced around 2134 ± 4 Ma (U-Pb zircon; Agyei-Duodu et al., 2009) and composed mainly of granite gneiss.

The Type 1 and Type 2 granitoids have all been intruded by the Type 3 and Type 4 granitoids. The Type 3 granitoids are composed of K-feldspar-rich granitoids, predominantly granite and monzonite, and intruded around 2106 ± 1 Ma. The Type 4 granitoids intruded around 2088 ± 1 Ma (U-Pb zircon dating by Hirdes et al. (1992)) and are composed of two mica or muscovite granites and minor granodiorite with local leucogranites (Fig. 2b). Mesozoic mafic dolerite dykes, inferred from aeromagnetic data, cut orthogonally across the granitoid complex. The dykes are made up mainly of dolerites, with minor

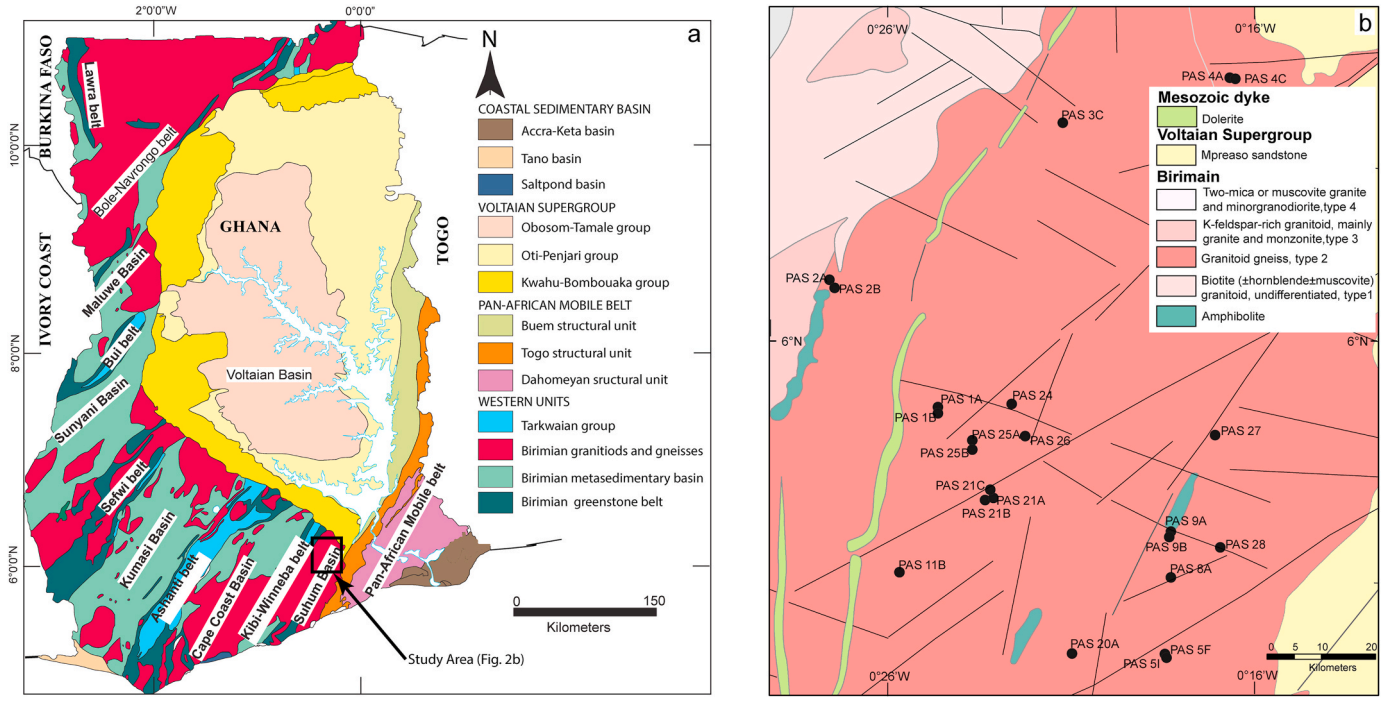

Fig. 2. **(a)** Simplified geological map of Ghana, showing the NE-SW trending greenstone belts of the Birimian terrane, and **(b)** a simplified geological map of the Suhum Basin illustrating different lithologies (modified after Agyei Duodu et al., 2009). The circular black dots represent sample locations.

gabbros, basalts, and subvolcanic rocks interbedded with minor volcaniclastics. Amphibolite, originating partially as a result of contact metamorphism, also outcrops sparsely within the Suhum Basin (Fig. 2b). These are Birimian protoliths that have been affected by Eburnean tectono-metamorphic overprinting (Agyei-Duodu et al., 2009).

3. Analytical methods

A total of 30 thin-sections were prepared for petrographic investigations, 24 polished thin-sections for mineral chemistry analysis, and 28 samples were prepared for whole-rock major and trace elements analysis.

3.1. Mineral chemistry

24 rock samples were carefully chosen for mineral chemistry analyses by the wavelength-dispersive spectrometry method using JEOL JXA8100 electron probe microanalyzer (EPMA). Measurements were carried out at an accelerating voltage of 15 kV, a beam current of 10 nA, a beam spot of 5 μm and 10–30 s counting time on peak. Standard calibration was done following the procedures of Su et al. (2014). The following natural mineral samples were selected and used for standard calibration; jadeite ($NaAlSiO_6$) for Na, Al and Si, rhodonite ($MnSiO_3$) for Mn, sanidine ($KAlSi_3O_8$) for K, garnet ($Fe_3Al_2Si_3O12$) for Fe, Cr-diopside (Mg, Cr) $CaSi_2O_6$ for Ca, and olivine (Mg, Fe)$_2SiO_4$ for Mg. Synthetic minerals namely rutile for Ti, 99.7% Cr_2O_3 for Cr, and Ni_2Si for Ni were also used. Matrix correlations were done using a program based on the ZAF procedure. Precisions of 98% and better were attained for all analysed elements.

3.2. Major and trace elements

Major and trace element compositions were obtained by X-Ray Fluorescence Spectrometry using the Shimadzu XRF-1500 instrument on fused glass disks and Inductively Coupled Plasma-Mass Spectrometry (ICP-MS) using the Agilent 7000a system respectively, at the Institute of Geology and Geophysics, Chinese Academy of Science (IGGCAS), Beijing, China, following the procedures described in Chu et al. (2009). Precision was better than 5%. For elements present in significant concentrations (>1 wt %.) and elements in low concentrations (<1 wt %), analytical uncertainties were 1–3% and ≈10% respectively.

4. Results

4.1. Field observations and petrography

Field observations and petrographical investigations made for the rocks within the Suhum Basin revealed the occurrence of four types of lithologies based on mineral assemblage, and texture. These are: (i) granite gneiss, (ii) migmatites, (iii) intrusive leucogranites, and (iv) mafic enclaves. A summary of the modal abundances of the major mineral phases in these lithologies is presented in Table 1.

4.1.1. Granite gneiss

The granite gneiss consists mainly of amphibole-bearing and biotite-bearing varieties. The amphibole-bearing gneiss occurs as huge plutons and inselbergs punctured throughout the study area. The amphibole-bearing gneiss is generally medium-to coarse-grained, weakly to strongly foliated, and exhibits typical compositional banding (Fig. 3a). It

Table 1
Estimated modal composition of the granitoid complex of the Suhum Basin.

Minerals (vol %)	Granite Gneiss	Intrusive Leucogranites	Migmatites	Mafic enclaves
Quartz	22–26	30–35	20–25	4–6
Plagioclase	18–23	25–30	25–30	20–22
Microcline	15–20	35–40	15–20	5–8
Orthoclase	4–8	–	–	5–10
Biotite	10–12	2–4	10–15	25–30
Muscovite	<1	<1	1	–
Amphibole	10–12	–	6–9	35–40
Epidote	<1	–	<1	<1
Titanite	<1	–	<1	–
Zircon	<1	<1	<1	–
Magnetite	–	<1	–	<1

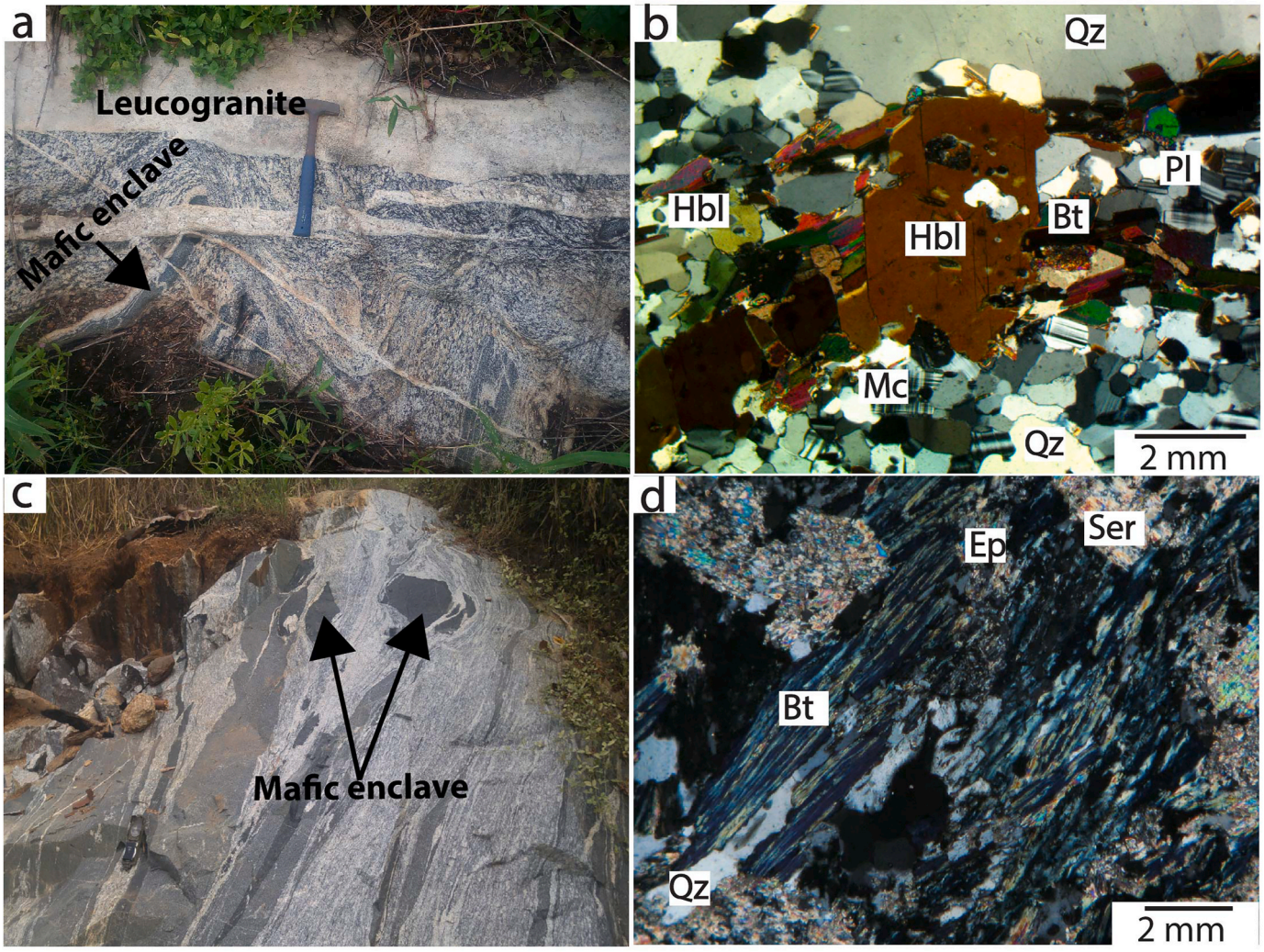

Fig. 3. Representative field photographs and photomicrographs of the studied granite gneiss. **(a)** amphibole-bearing gneiss with leucogranite dykes and mafic enclaves **(b)** amphibole-bearing gneiss showing foliation defined by the amphiboles, cross polars (XPL) **(c)** Biotite gneiss with mafic enclaves; and **(d)** elongated and fragmented mineral grains showing sub-parallel arrangement due to shearing, cross polars (XPL).

is composed predominantly of quartz and plagioclase, together with microcline, orthoclase, hornblende, and biotite. Quartz shows undulose extinction and occurs in some cases as blebs in the hornblende and microcline (Fig. 3b). The amphibole-bearing gneiss is cross-cut by veins and dykes of pegmatite and leucogranites, which are easily recognisable by their sharp contacts (Fig. 3a).

The biotite-bearing gneiss is light grey and coarse-grained (Fig. 3c). The mineral constituents include microcline, quartz, plagioclase, biotite, and muscovite, with accessory phases of epidote, zircon, and opaque minerals (Fig. 3d). Microcline occurs as coarse, deformed, and fractured irregular grains. Plagioclase is mostly tubular and appears severely sericitized (Fig. 3d). Biotite is mostly acicular, interstitial, and shows preferred orientation, and is partially altered to chlorite. Quartz occurs as anhedral, irregular sub-grains and appears as blebs in some phases of microcline.

4.1.2. *Migmatites*

The migmatites are largely characterised by layered sub-parallel or stromatic segregations of quartzo-feldspathic domains flanked by biotite-hornblende rich melanosomes and mesosomes of varying thickness (Fig. 4a). The migmatites are composed of biotite, amphibole, plagioclase, microcline, and minor quartz, with accessory phases of titanite and magnetite (Fig. 4b). Biotite occurs as intergrowths into phases of hornblende which are oriented sub-parallel to the foliation. Quartz mostly appears as rounded blebs on the surface of the ferromagnesian minerals and microcline. Generally, melanosomes contain mineral assemblages akin to those of amphibole-bearing gneiss, but with higher abundances of amphibole and biotite. The leucosomes are coarse-grained, inequigranular, dominated by plagioclase and microcline, with subordinate amounts of quartz and traces of biotite.

4.1.3. *Intrusive leucogranite*

The leucogranite occurs as dykes with varying thicknesses which ubiquitously intrude the granitic gneiss and migmatites (Fig. 4c). The leucogranite is medium-to coarse-grained, generally with interlocking equigranular mineral grains. It is composed predominantly of K-feldspar, plagioclase, and quartz, with minor amounts of biotite and muscovite (Fig. 4d). Biotite has a dark green to brown colour and occurs as individual grains and aggregates which appear partially chloritized and interstitial. Quartz occurs sutured, often showing grain boundary migration, and also as rounded blebs in the feldspars. Plagioclase exhibits worm-like vermicules of quartz culminating in mymerkitic textures, which are quite common.

4.1.4. *Mafic enclave*

The mafic enclaves usually occur as dark mafic layers hosted in the

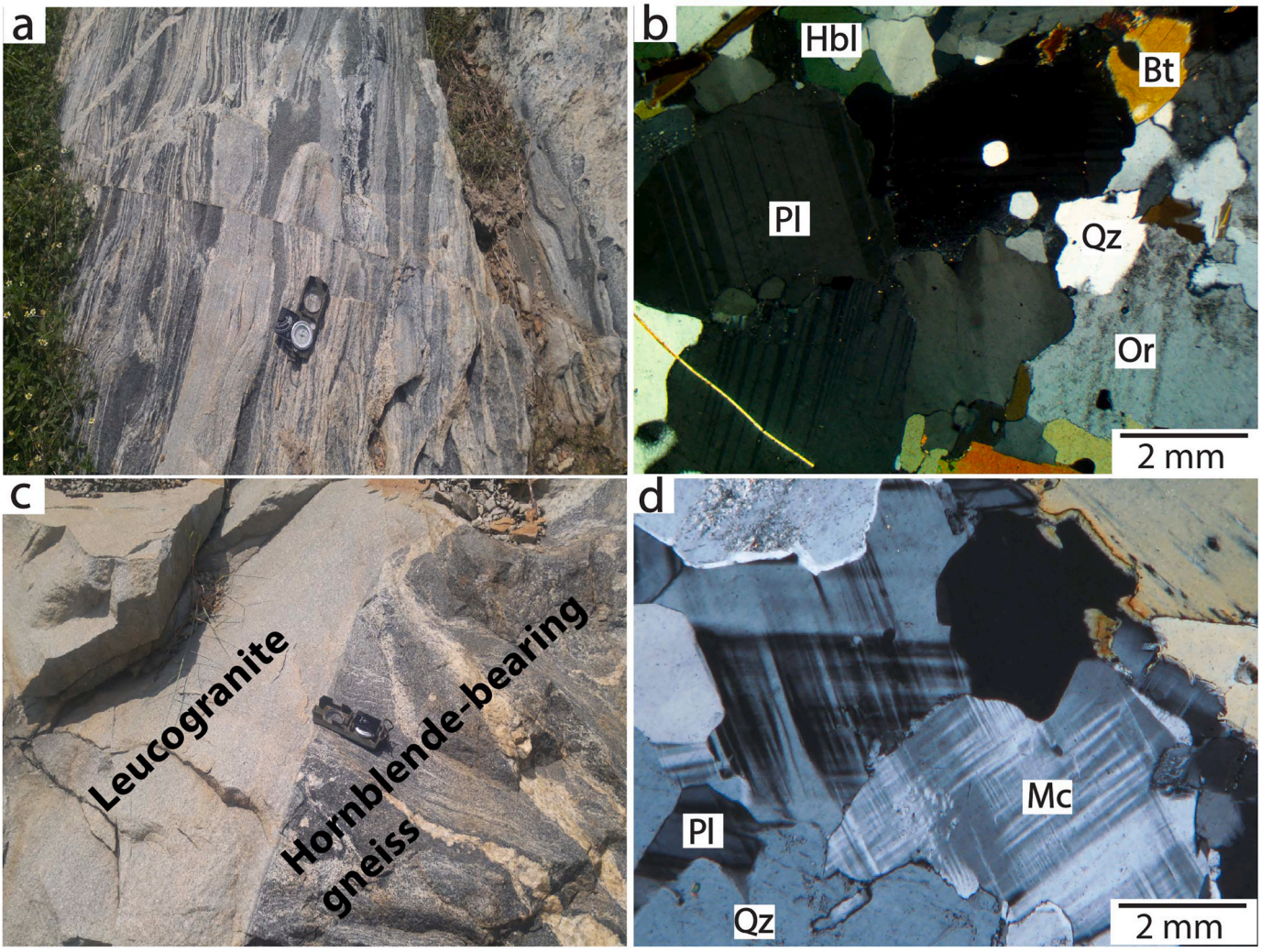

Fig. 4. **(a)** Stromatic layering of layer-parallel in-situ leucosomes and adjacent melanosomes and mesosomes; **(b)** migmatite showing coarse-grained plagioclase and orthoclase with interstitial and blebs of quartz, XPL **(c)** field photograph of leucogranites, and **(d)** photomicrograph of leucogranite showing the interlocking texture of microcline, quartz, and plagioclase. Note: the worm-like overgrowth of quartz (myrmekites) in plagioclase, XPL.

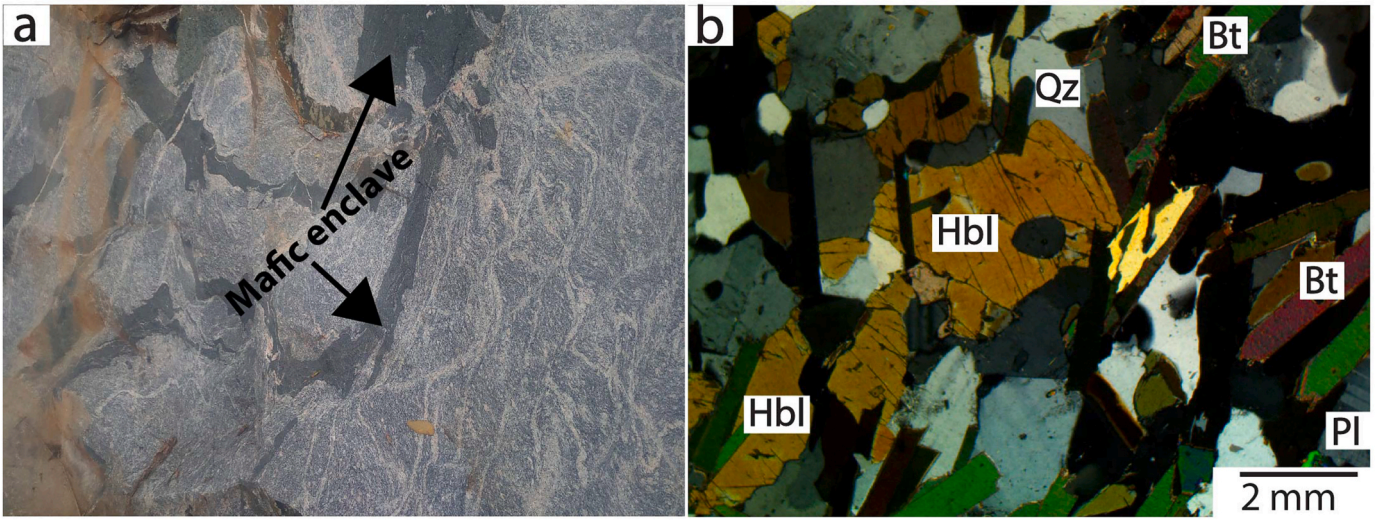

Fig. 5. **(a)** Field photo of mafic enclaves **and (b)** photomicrograph of mafic enclave, under cross polars.

granite gneiss (Fig. 5a). They appear as deformed layers of country rocks that were remobilised and partly assimilated by the intruding granitoids (Fig. 5a). Occasionally, the mafic enclaves are rounded and/or ellipsoidal enclaves. They are mostly concordant with the principal foliation direction and show faulting and folding in some areas. Their contact with the host granite gneiss is often sharp and marked by rims of biotite minerals. The mafic enclaves are medium-to coarse-grained and display a generally schistose structure. The minerals observed include biotite, hornblende, plagioclase, K-feldspar, and quartz (Fig. 5b). Hornblende is mostly anhedral to subhedral, skeletal, and appears altered to epidote. Biotite occurs as blade-like mineral grains which overgrow other mineral phases. Chlorites are present in minor amounts. Quartz is mostly interstitial, irregular grain, that exhibits undulose extinction. Accessory phases include epidote and magnetite.

4.2. Mineral chemistry

4.2.1. Biotite

The chemical formula of biotite was calculated based on the 22-cation charge (Supplementary Table S1). Based on the 10 × TiO_2-FeO*-MgO ternary diagram (Fig. 6a), Nachit et al. (2005) proposed that biotite can be grouped into magmatic (primary) types, re-equilibrated types, and neo-formed types. The leucogranite and mafic enclave biotites, respectively, comprise mainly primary and re-equilibrated biotite types (Fig. 6a). In the $Fe_t/(Fe_t + Mg)$ vs. Total Al plot, the studied biotite minerals plot mainly in the annite-siderophyllites species, with a few trending towards the phlogopite species (Fig. 6b).

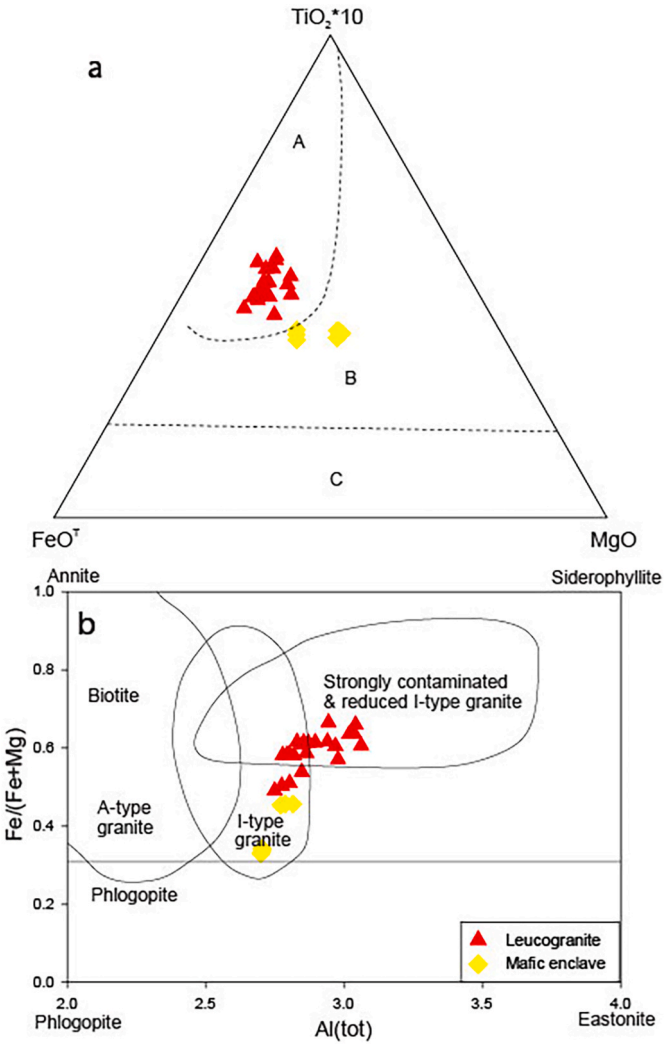

Fig. 6. (a) Biotite ternary plot of 10 × TiO_2-MgO-FeO* after Nachit et al. (2005). A-magmatic, B-recrystallised and C-neo-formed; **(b)** Al (tot) vs. Fe/Fe + Mg diagram (after Howie et al., 1992).

4.2.2. Feldspar (plagioclase and K-feldspar)

Supplementary Table S2 presents the chemical composition of the feldspars. Plagioclase shows high amounts of albite (Ab_{86-67}) relative to anorthite (An_{13-32}) and orthoclase ($Or_{0.4-1.9}$) indicating strictly oligoclase to andesine composition (Fig. 7a). K-feldspar shows high amounts of orthoclase (Or_{89-99}) relative to anorthite ($An_{0-0.2}$) and albite ($Ab_{0.8-11}$) indicating a strictly microcline to orthoclase composition (Fig. 7b). Overall, the plagioclase in the granitic gneiss has anorthite (An_{15-31}), that for the leucogranite in An_{13-28}. For the migmatites and mafic enclaves, the anorthite contents are An_{23-25}, and An_{19-23} respectively. In terms of K-feldspar, orthoclase is Or_{89-99} in the gneiss, Or_{94-97} in the leucogranite, Or_{92-96} in the migmatite and Or_{99} in the mafic enclaves.

4.2.3. Amphibole

The structural formula of the amphiboles was calculated on an anhydrous basis, assuming 23 oxygen atoms per half unit *(apfu)* cell (Supplementary Table S3). The amphiboles fall within the magnesio-hornblende (granitic gneiss, migmatite and mafic enclave) and tschermakite (granitic gneiss) fields for $(Na + K)_A < 0.5$ (Fig. 8a) and in the ferro-edenite (granitic gneiss), magnesio-hastingsite (granitic gneiss, mafic enclave) and ferro-pargasite (granitic gneiss) field for $(Na + K)_A > 0.5$ (Fig. 8b; Leake et al., 1997). According to the Na_B vs. $(Ca + Na)_B$ classification diagram after Leake et al. (1997), the amphiboles belong to the calcic (all rock-types) group (Fig. 8c). The $Ca + Al^{IV}$ (apfu) vs. Si + Na + K (apfu) diagram (Giret et al., 1980) indicates that the granitic gneiss, migmatites and mafic enclave amphiboles are mostly primary magmatic-hornblende, with the exception of amphiboles from one sample of the mafic enclave, which plot in the secondary actinolite-hornblende field (Fig. 8d).

4.3. Whole-rock major and trace elements

4.3.1. Granite gneiss

The granite gneiss records intermediate to high SiO_2 and K_2O contents in a range of 58.28–72.58 wt% and 0.86–5.97 wt% respectively (Table 2). They are mostly metaluminous to weakly peraluminous, as shown in Fig. 9a (Shand, 1943; Maniar and Piccoli, 1989). On the feldspar normative An-Ab-Or diagram (O'Connor, 1965), the granite gneisses plot mainly in the tonalite-trondhjemite field, with two samples plotting in the granite field (Fig. 9b). They form a linear trend ranging from diorite through granodiorite to granite in the total alkali versus silica (TAS) classification diagram (Fig. 9c) after Middlemost (1994). The granite gneiss generally has calc-alkaline magmatic signatures and plots in the medium-to high-K calc-alkaline series field of the K_2O vs. SiO_2 diagram and mainly in the magnesian field on the $FeO_t/(FeO_t + MgO)$ vs. SiO_2 diagram, Fig. 9d–f (Peccerillo and Taylor, 1976; Frost and Frost, 2008). On the chondrite normalised REE diagrams after Palme and O'Neill (2014), the granite gneiss shows varying degrees of HREE depletion (La_N/Yb_N between 4.19 and 57.73) and varying Eu anomalies (Eu/Eu* = 0.58–2.05; Fig. 10a). In the primitive mantle-normalised spider diagram, they are characterised by enrichment of LILE and the depletion of HFSE (Fig. 10b).

4.3.2. Migmatites

The migmatites are mainly metaluminous (Fig. 9a) and show affinity for tonalite on the feldspar normative An-Ab-Or diagram (Fig. 9b). They plotted in the field of granodiorite and diorite, with one sample straddling the boundary line between granodiorite and granite on the TAS diagram (Fig. 9c). On Fig. 9d–f, the migmatites plot as calc-alkaline, low to medium K-tholeiites, and magnesian. The chondrite-normalised plot after Palme and O'Neill (2014) for the studied migmatites (Fig. 10c)

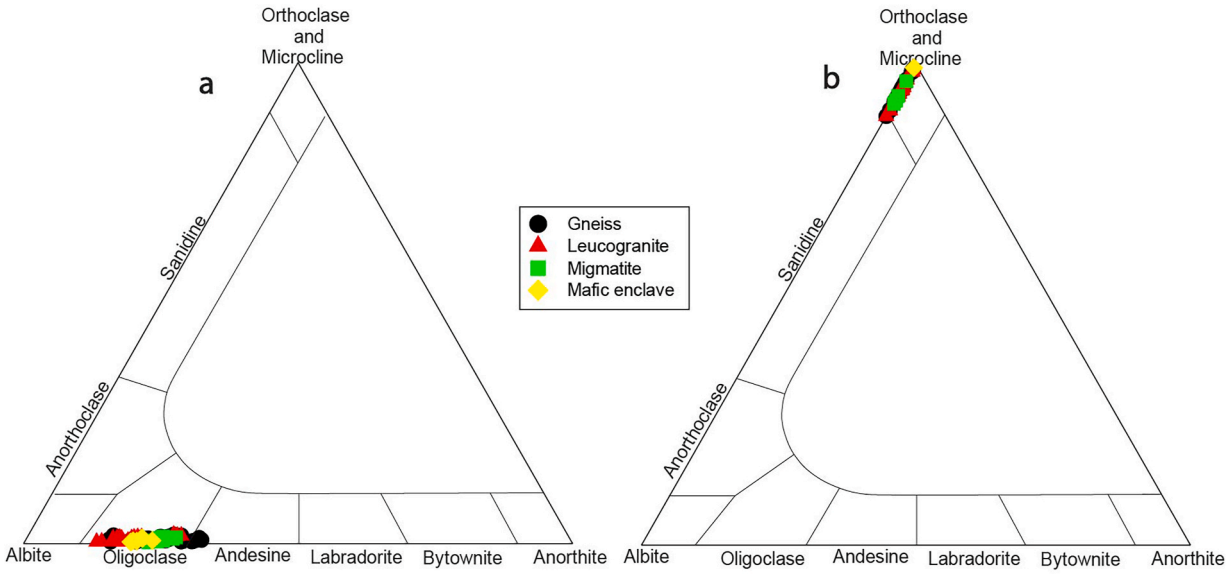

Fig. 7. Or–Ab–A ternary diagram of felspar (after Howie et al., 1992) **(a)** plagioclase and **(b)** K-feldspar. Note: The samples from the granitoids complex of the Suhum Basin plot mainly as oligoclase, and microcline-orthoclase, respectively.

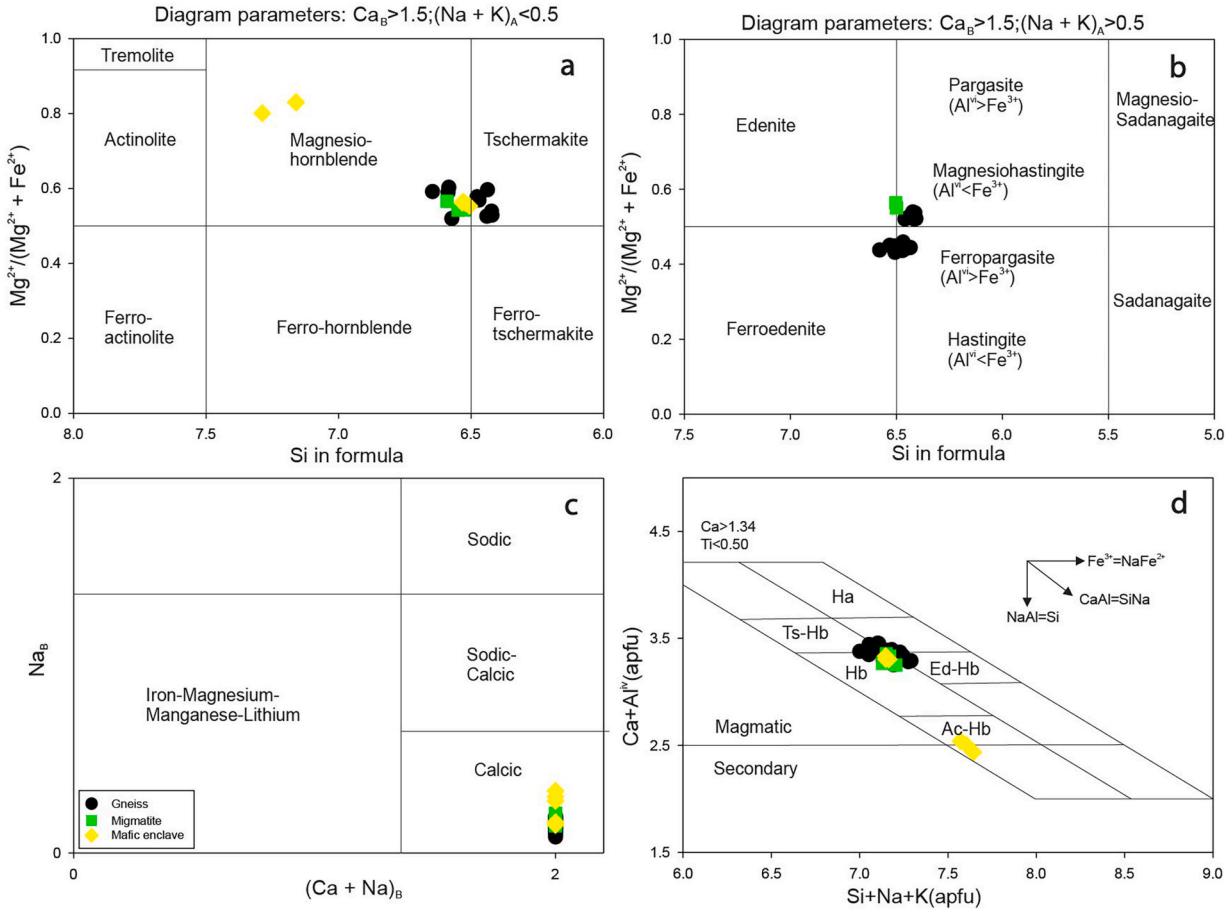

Fig. 8. **(a)** Amphibole classification diagram based on low $(Na + K)_A$ content (Leake et al., 1997); **(b)** Amphibole classification diagram based on higher $(Na + K)_A$ content (Leake et al., 1997); **(c)** The composition of the amphiboles (Leake et al., 1997); and **(g)** $Ca + Al^{IV}$ vs. $Si + Na + K$ diagram (Giret et al., 1980).

displays LREE enrichment and a nearly flat HREE pattern (La_N/Yb_N ratios between 5.22 and 59.89). The migmatites show slightly pronounced negative and positive Eu anomalies ranging from 0.76 to 2.28. The leucosome and melanosome segregates (from samples PAS 9 A and 9 B, respectively) exhibit similar REE patterns, but the melanosome has higher REE enrichment (about 10× folds) than the leucosome (Fig. 10c). They display pronounced positive (melanosome segregate) and negative (leucosome segregate) Eu anomalies and more pronounced HREE

Table 2
Major and trace element analyses for representative samples from the Suhum Basin granitoid complex.

Granite Gneiss													
SAMPLE NAME (1–29)	PAS 1 A	PAS 2 A	PAS 2 B	PAS 3C	PAS 5I	PAS 8 A	PAS 16 A	PAS 19 B	PAS 21 A	PAS 24	PAS 25 A	PAS 26	PAS 4 A
SiO_2	70.27	70.45	69.03	65.58	72.58	58.73	66.41	64.63	70.36	58.28	58.78	67.83	66.84
TiO_2	0.24	0.3	0.34	0.86	0.33	0.85	0.57	0.6	0.26	1.35	0.89	0.65	0.3543
Al_2O_3	15.98	15.48	16	14.79	13.6	13.43	15.02	14.79	15.55	15.96	18.04	15.91	13.17
Fe_2O_3t	1.94	2.41	2.41	5.63	2.52	8.6	4.88	5.65	2.45	7.26	5.34	3.22	3.33
MnO	0.04	0.06	0.06	0.1	0.06	0.15	0.1	0.1	0.05	0.12	0.09	0.05	0.08
MgO	1.07	0.84	0.88	1.77	0.56	4.81	2.16	2.36	0.58	3.68	2.82	1.13	1.1
CaO	3.42	2.41	2.42	4.64	1.38	6.89	5.08	5.57	2.87	7.17	6.71	3.6	4.01
Na_2O	5.66	5.05	5.27	4.08	2.71	3.17	4.28	4.04	4.97	3.99	4.98	4.91	3.403
K_2O	0.86	3.16	3.11	1.84	5.97	1.9	1.33	1.28	2.01	1.31	1.07	1.62	3.8773
P_2O_5	0.15	0.11	0.16	0.22	0.12	0.09	0.29	0.42	0.11	0.54	0.4	0.37	0.12
LOI	0.28	0.16	0.22	0.46	0.28	1	0.24	0.3	0.12	0.4	0.38	0.42	3.53717
TOTAL	99.91	100.42	99.9	99.96	100.11	99.62	100.36	99.75	99.33	100.05	99.49	99.7	99.82177
Sum	99.63	100.27	99.68	99.51	99.83	98.62	100.12	99.44	99.21	99.66	99.12	99.29	96.2846
Cr	19.8	32.1	3.5	38.9	17.8	52.5	48.6	24	18.2	77.6	72.4	6.2	41.4
Ni	17.2	19.2	16.3	23	8.8	70.7	42.2	37.7	9.5	42.2	38.6	4.3	24.8
Sr	760.4	825.1	960.9	298.3	266.6	197.7	402.7	434.4	697.3	688.1	849.2	825.1	234.1
V	42.1	54.7	34	94.6	20.6	157.8	75.6	88.1	19.2	115.1	82.1	35.1	38.5
Sc	4.13	3.61	3.73	13.86	3.6	23.58	13.6	15.98	2.58	19.06	14.19	3.99	5.293
Rb	29.97	80.86	95.81	75.96	123.51	66.07	47.42	46.87	35.17	36.4	25.68	48.45	88.807
Sr	740	780	925	295	254	205	393	436	694	685	807	821	190
Y	2.4	4.88	5.67	37.65	21.32	19.97	27	22.08	2.44	25.79	22.3	4.88	7.686
Zr	111.18	133.7	129.84	284.41	265.29	121.38	295.28	184.21	113.6	539.54	210.88	350.13	126.833
Nb	2.76	8.62	11.64	20.33	9.71	9.24	17.75	12.53	2.78	15.43	12	5.18	4.842
Cs	4.35	2.97	5.68	4.45	2.37	1.57	2.53	1.9	2.55	1.59	1.63	1.66	3.119
Ba	559	1082	1349	736	1823	526	693	918	1280	737	692	1121	836
La	8.88	36.86	38.7	51.08	81.33	13.81	30.57	60.72	11.46	31.82	24.76	41.96	21.206
Ce	16.1	59.67	66.83	92.96	140.28	29.47	59.62	113.48	19.1	74.63	58.11	72.66	32.157
Pr	2.13	6.43	7.54	10.95	14.84	3.86	7.62	12.97	2.34	11	9.02	9.07	3.808
Nd	8.08	20.26	24.88	42.94	48.37	15.59	30.45	48.03	8.6	45.55	39.52	33	13.546
Sm	1.43	3.02	3.96	8.39	7.16	3.24	6.03	7.57	1.35	9.53	8.79	5.03	2.136
Eu	0.6	0.82	0.99	2.18	1.24	1.01	1.74	1.97	0.8	2.77	2.7	1.45	0.732
Gd	1.1	2.3	2.73	7.79	6.01	3.37	5.57	6.36	1.05	7.63	6.87	3.14	1.935
Tb	0.13	0.24	0.3	1.23	0.82	0.57	0.87	0.83	0.12	1.06	0.97	0.3	0.261
Dy	0.6	1.08	1.3	6.99	4.27	3.46	5	4.24	0.6	5.52	4.9	1.23	1.307
Ho	0.11	0.19	0.24	1.47	0.83	0.76	1.06	0.86	0.12	1.06	0.93	0.22	0.261
Er	0.28	0.48	0.58	3.94	2.14	2.1	2.88	2.28	0.28	2.72	2.29	0.51	0.74
Tm	0.04	0.07	0.08	0.58	0.31	0.33	0.43	0.34	0.04	0.37	0.31	0.07	0.111
Yb	0.23	0.43	0.49	3.69	1.98	2.22	2.84	2.21	0.23	2.4	1.92	0.49	0.756
Lu	0.04	0.07	0.08	0.55	0.28	0.34	0.43	0.34	0.04	0.36	0.27	0.09	0.122
Hf	2.92	3.36	3.28	7.48	7.42	3.49	8.29	5.12	3.28	13.42	5.38	9.27	3.706
Ta	0.11	0.47	0.83	1.76	1.98	0.95	1.93	0.86	0.12	0.81	0.56	0.14	0.263
Pb	4.82	17.18	19.44	10.96	29.4	6.12	7.8	10.12	9.86	5.52	6.28	9.24	7.635
Th	0.39	6.13	6.37	11.05	27.87	2.37	5.04	11.59	0.95	0.97	0.86	7.29	6.07
U	0.56	1.93	2.46	2.7	2.07	0.72	1.1	0.99	0.26	0.68	0.37	0.59	0.461

	Intrusive Leucogranite								Migmatite				Mafic enclaves		
SAMPLE NAME	PAS 5 F	PAS 5H	PAS 11 B	PAS 16 B	PAS 19 A	PAS 20 A	PAS 21 B	PAS 25 B	PAS 9 A	PAS 15 A	PAS 27	PAS 9 B	PAS4C	PAS 5C	PAS 21C
SiO2	81.79	72.91	70.75	72.77	74.28	73.94	71.96	75.05	71.02	69.37	64.46	59.85	51.5	54.47	58.29
TiO2	0.04	0.2	0.22	0.23	0.08	0.16	0.08	0.04	0.18	0.49	0.64	1.11	0.57	1.06	0.99
Al2O3	9.38	14.24	16.13	13.77	13.64	14.06	16.16	14.12	15.92	14.43	14.69	15.51	9.93	17.15	15.97
Fe2O3t	0.57	1.69	2.06	2.11	1.25	1.59	0.87	1.12	1.54	3.96	6.86	6.87	10.27	8.13	7.36
MnO	0.04	0.04	0.05	0.06	0.03	0.06	0.03	0.07	0.04	0.08	0.12	0.09	0.18	0.14	0.16
MgO	0.1	0.31	0.63	0.3	0.19	0.32	0.13	0.08	1.03	1.23	2.3	3.19	13.65	3.61	3.47
CaO	1.01	1.49	2.4	1.25	1.13	1.31	2.56	0.86	3.65	4.08	4.65	5.95	8.25	6.92	6.57
Na2O	2.53	3.04	5.39	3.22	3.35	3.73	5.25	4.26	5.37	4.37	4.43	4.09	1.99	4.45	4.28
K2O	3.59	5.81	2.21	5.48	5.39	4.92	2.42	4.8	0.76	1.07	1.09	1.78	1.89	2	1.62
P2O5	0.01	0.05	0.09	0.1	0.03	0.04	0.03	0.02	0.09	0.19	0.29	0.89	0.4	0.82	0.58
LOI	0.26	0.66	0.22	0.2	0.34	0.4	0.14	0.16	0.22	0.32	0.4	0.86	0.82	0.6	0.52
TOTAL	99.31	100.44	100.16	99.49	99.7	100.52	99.62	100.58	99.82	99.6	99.92	100.18	99.46	99.34	99.81
Sum	99.06	99.78	99.93	99.29	99.37	100.13	99.49	100.42	99.6	99.27	99.53	99.33	98.63	98.75	99.29
Cr	9.3	20.2	9.3	14.5	11.1	13.9	21.5	13	39	24.6	35.5	54.7	819.1	24.5	31.5
Ni	5.9	7.5	8.3	10.9	8.6	10.6	7.1	5.8	41.9	15.8	29.4	31.6	166.6	23.3	21.3
Sr	75.6	202.2	771.7	191.9	157.9	159.8	1405.8	171.4	748.5	358.5	531.1	767	359.3	626.8	922
V	0	28.5	32.1	43	3.3	12.9	47.2	17.9	30.3	60.7	95.3	129	176.5	153.8	144.6
Sc	1.069	2.91	3.04	4.09	1.57	2.87	1.16	2.33	1.62	5.31	16.56	14.55	31.63	23.55	21.19
Rb	104.326	102.94	52.82	133.02	126.05	146.39	23.25	146.69	15.15	47.19	20.18	57.48	64.65	61.49	53.17
Sr	72	187	655	182	138	160	1096	170	681	317	522	746	337	636	909
Y	4.85	7.45	5.76	7.07	1.63	12.77	2.56	9.69	1	11.5	14.78	16.91	16.78	58.07	27.32
Zr	1.253	130.39	75.7	229.05	83.66	119.27	58.05	50.57	63.28	155.64	424.32	325.24	88.58	228.62	151.24
Nb	1.741	13.16	4.39	6.91	2.38	14.79	1.82	9.78	1.09	7.17	6.41	10.92	3.87	15.15	9.76

(*continued on next page*)

Table 2 (*continued*)

	Intrusive Leucogranite								Migmatite				Mafic enclaves		
SAMPLE NAME	PAS 5 F	PAS 5H	PAS 11 B	PAS 16 B	PAS 19 A	PAS 20 A	PAS 21 B	PAS 25 B	PAS 9 A	PAS 15 A	PAS 27	PAS 9 B	PAS4C	PAS 5C	PAS 21C
Cs	2.313	1.06	9.53	2.17	1.61	2.23	0.83	1.68	0.5	2.3	1.95	2.73	4.17	1.3	5.16
Ba	90	1189	1284	1218	669	1085	1692	892	402	502	529	1119	396	1397	1124
La	1.465	31.96	14.48	54.3	8.14	97.75	6.8	10.07	10.66	23.45	11.62	82.03	14.71	57.89	37.73
Ce	1.116	52.08	27.32	98.57	13.76	178.92	10.9	18.71	17.14	41.5	23.43	162.93	32.31	118.07	79.55
Pr	0.165	5.64	3.58	11.24	1.71	19.31	1.38	2.4	1.94	4.77	3.38	18.81	4.61	15.45	10.75
Nd	0.741	18.35	13.73	38.14	6.22	65.72	4.69	9.34	6.87	17.77	14.86	69.64	19.12	63.46	42.84
Sm	0.311	2.97	2.31	5.39	1.23	10.9	0.77	2.01	0.92	3.01	3.74	9.87	4.22	13.87	9.05
Eu	0.202	0.5	0.62	0.73	0.41	0.88	0.49	0.35	0.59	0.95	1.01	2.13	1.16	3.14	2.3
Gd	0.446	2.36	1.81	3.97	0.93	8.41	0.61	1.78	0.68	2.79	3.58	7.39	3.85	13.03	7.34
Tb	0.099	0.32	0.24	0.42	0.11	0.95	0.07	0.29	0.07	0.4	0.56	0.82	0.58	2.03	1.04
Dy	0.661	1.46	1.22	1.65	0.49	3.67	0.35	1.61	0.32	2.2	3.09	3.57	3.22	11.55	5.44
Ho	0.148	0.26	0.24	0.26	0.08	0.53	0.08	0.33	0.06	0.46	0.6	0.64	0.66	2.34	1.08
Er	0.395	0.64	0.64	0.66	0.2	1.01	0.26	0.87	0.14	1.21	1.59	1.62	1.8	6.34	2.83
Tm	0.05	0.1	0.09	0.1	0.03	0.11	0.05	0.13	0.02	0.17	0.23	0.23	0.27	0.89	0.4
Yb	0.293	0.69	0.61	0.64	0.18	0.61	0.36	0.88	0.12	1.09	1.5	1.4	1.72	5.62	2.58
Lu	0.043	0.11	0.11	0.11	0.03	0.08	0.06	0.14	0.02	0.17	0.22	0.21	0.26	0.84	0.39
Hf	0.084	4.49	1.93	6.81	3.21	4.24	1.71	2.19	1.75	4.38	11.08	7.83	2.5	6.57	4.31
Ta	0.231	1.42	0.21	0.32	0.17	0.65	0.17	0.96	0.03	0.4	0.29	0.51	0.2	0.95	0.58
Pb	22.767	27.28	14.01	33.79	24.63	37.99	13.37	25.83	4.46	6.67	3.81	8.14	3.93	9.4	8.81
Th	1.637	20.27	3.25	13.94	8.64	56.3	1.05	2.9	0.59	3.39	0.07	7.86	1.45	6.11	2.92
U	22.909	3.15	0.68	1.88	3.64	6.12	0.62	2.94	0.18	0.82	0.28	1.51	0.5	1.33	0.83

depletions. Fig. 10d shows a plot of the migmatites normalised against primitive mantle (Palme and O'Neill, 2014). On this plot, the migmatites show positive Ba, strong negative HFSE (Nb, Ta, Ti), and variable Sr anomalies (Fig. 10d). They exhibit strong negative P anomalies as well as positive Pb anomalies. However, the leucosome shows moderately positive Ba and Sr anomalies, while the melanosome shows depletions in these elements.

4.3.3. Intrusive leucogranite

The leucogranites are slightly peraluminous (Fig. 9a), plot as granite on both the feldspar normative An-Ab-Or and TAS diagrams (Fig. 9b and c), after O'Connor (1968) and Middlemost (1994) respectively and show a calc-alkaline signature (Fig. 9d). They spread from the medium-K calc-alkaline to the shoshonitic fields and dominantly in the ferroan field, with one sample plotting in the magnesian field (Fig. 9e and f). On the chondrite-normalised plot after Palme and O'Neill (2014), the LREE are enriched relative to the HREE (La_N/Yb_N between 7.71 and 108.04; Fig. 10e). The leucogranites show predominantly negative Eu anomalies ranging from 0.28 to 1.17 (except for one sample, which has an Eu/Eu* value of 2.19). The leucogranites normalised against primitive mantle (Palme and O'Neill, 2014) show positive Ba and La, strong negative HFSE (pronounced Nb-Ta troughs, strong Ti anomaly), and variable Sr anomalies (Fig. 10f). They also present strong negative P anomalies as well as positive Pb anomalies.

4.3.4. Mafic enclave

Samples from the mafic enclave exhibit trondhjemite and granodiorite compositions (Fig. 9b). On the TAS classification diagram (Fig. 9c), the mafic enclave samples fall within the diorite and gabbro diorite fields. They also plot within the calc-alkaline and medium-to-high calc-alkaline fields on the AFM, K_2O vs. SiO_2, and Na_2O vs K_2O diagrams (Fig. 9d–f). The mafic enclave samples display LREE enrichment and a nearly flat but slightly enriched HREE pattern (La_N/Yb_N between 4.01 and 9.86; Fig. 10g). These rocks show a somewhat negative Eu anomaly (Eu/Eu* ranging from 0.71 to 0.88). In the primitive-mantle normalised (Sun and McDonough, 1989) plots (Fig. 10h), they show positive spikes in Rb, Ba, and Pb, slight depletions in Th and Zr, and negative Nb, Ta and Ti anomalies.

4.4. Physical conditions of granitoid magmas

From field observations and petrographic studies of the granitoid complex of the Suhum Basin, all the granitoids encountered comprise biotite, hornblende, K-feldspar, plagioclase, and quartz as its major mineral constituents. Over the years, these minerals have been used to determine the P-T conditions for the formation of granitoid rocks (Andersson et al., 2011). Several studies have shown that hornblende is the most common amphibole in most calc-alkaline granitoids in cratonic environments whose formation is typified by extensional rift and subduction zone magmas (Pitcher, 1997; Bucher and Frey, 2002) and also a good indicator of temperature and pressure over a wide range of metamorphic conditions (Plyusnina, 1982). The reason why the mineral hornblende was used to determine the thermobarometry conditions for the formation of the Suhum basin rocks is that, from empirical studies, its total Al(Al^{tot}) and tetrahedral Al (Al^{iv}) content per 23 oxygen forms linear trends (Hammarstrom and Zen, 1986) that show that Al in hornblende varies with the pressure of crystallisation and thereby provides a means to determine the depth of emplacement (Schmidt, 1992; Sepahi et al., 2012). Also, the solidus pressure from which these granitoids in the Suhum basin are formed is dependent on several equations by Hammarstrom and Zen (1986), Hollister et al. (1987), Johnson and Rutherford (1989), and Schmidt (1992), where the Al content in the hornblende allows for the determination of the equilibrium pressure and temperature. This is so because the variation of Al in hornblende is a function of temperature. These calculations are therefore dependent on the phase rule and the varying equilibrium phases of Al in hornblende (Schmidt, 1992). The following equation below was used by the authors to estimate the solidus pressures of the calc-alkaline granitoid rocks in the Suhum basin.

(1) P (±3 kbars) = −3.92 + 5.03 Al^{tot} (after Hammarstrom and Zen, 1986).

By enlarging the Al calibration dataset, Hollister et al. (1987), proposed similar equations with reduced errors.

(2) P (±1 kbar) = −4.76 + 5.64 Al^{tot} with r^2 = 0.97 (after Hollister et al., 1987).
(3) P (±0.5 kbar) = −3.01 + 4.7 Al^{tot} (Schmidt, 1992).

Schmidt calibrated the Al in hornblende using pressures between 2 and 13 kbars and a temperature range between 660 and 750 °C under water saturated conditions.

Numerical calculations from mineral chemistry data of the granite

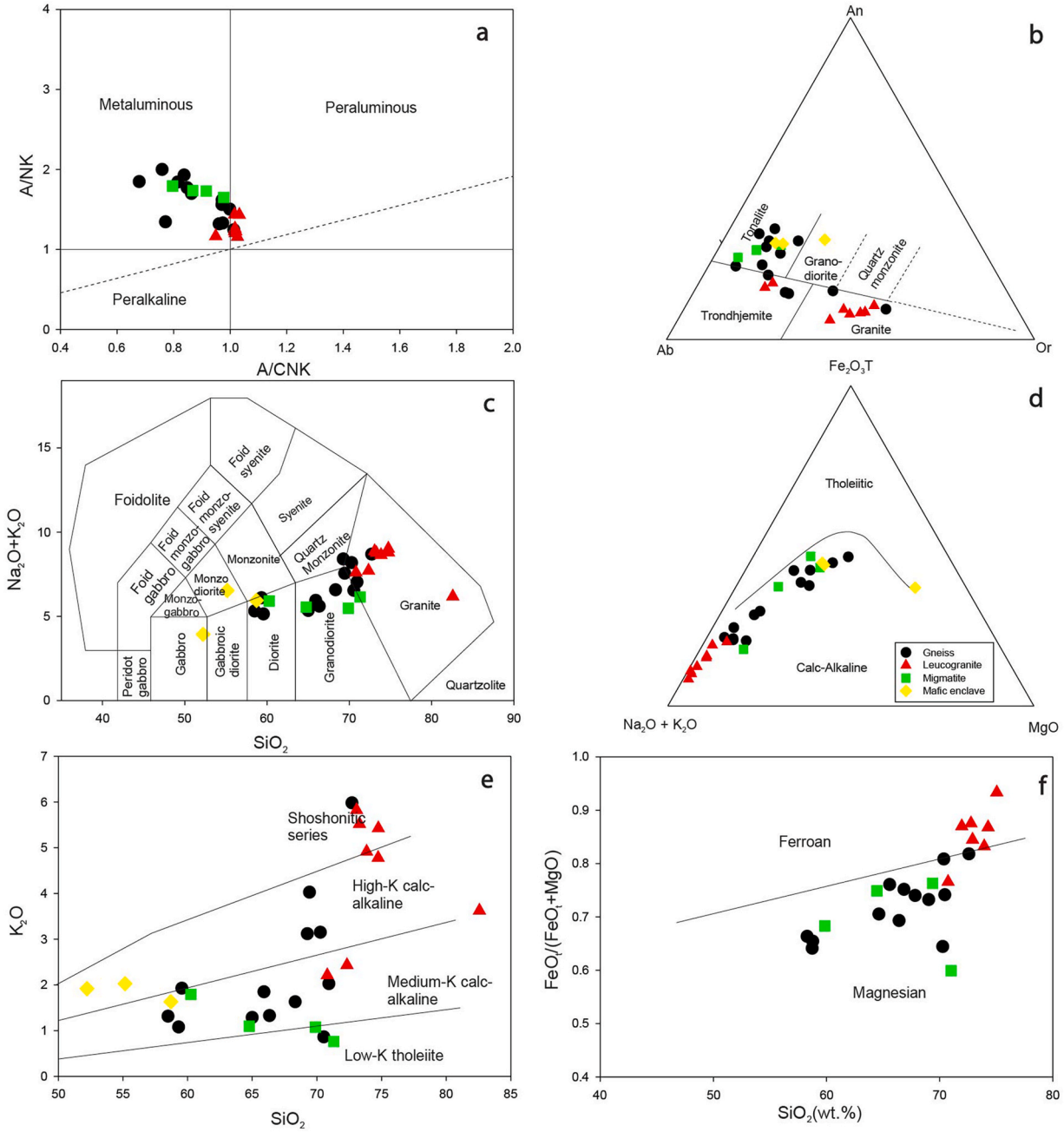

Fig. 9. Major element classification diagrams of the Suhum Basin granitoid complex **(a)** Plot of A/CNK (molar $Al_2O_3/(CaO + Na_2O + K_2O)$) vs. ANK (molar $Al_2O_3/(Na_2O + K_2O)$) (Maniar and Piccoli, 1989); **(b)** Or-Ab-An ternary diagram (O'Connor, 1965); **(c)** Total alkalis vs silica (TAS) (Middlemost, 1994); **(d)** AFM diagram (Irvine and Baragar, 1971); **(e)** K_2O vs. SiO_2 diagram (after Peccerillo and Taylor, 1976); and **(f)** SiO_2 vs. $FeO_t/(FeO_t + MgO)$ diagram (after Frost and Frost, 2008).

gneiss yielded temperatures and pressures of ~633–712 °C at 5.2–7.2 kbar, respectively. The migmatites recorded temperatures of ~676–698 °C and pressures of ~5.7–6 kbar. The mafic enclave samples yielded P-T estimates of ~662–667 °C at 6.1 kbar with the exception of one sample, which recorded P-T estimates of ~573–610 °C at ~2.0–2.5 kbar (Supplementary Table S5).

Because the Ti solubility in biotite is dependent on temperature, a high content of Ti may connote a high temperature (Esfahani et al., 2017). The TiO_2 contents of biotite in the studied rock samples range from 0.97 to 3.58 wt% (granite gneiss), 2.21–3.50 wt% (leucogranites), 1.83–2.92 wt% (migmatites), and 1.73–1.91 wt% (mafic enclaves), suggesting intermediate to high temperatures during crystallisation. On the plot of Ti vs. Mg/(Mg + Fe) (Fig. 11c), the granite gneiss has temperatures between 450 and 700 °C, the intrusive leucogranite and migmatites plot in the temperature range of 600–700 °C, and the mafic enclave samples have temperatures between 600 and 650 °C. These values suggest high crystallisation temperatures for the rocks of the Suhum basin. The low temperatures, 450 °C could be the effect of metamorphism of the rocks.

4.4.1. *Depth of magma emplacement*

Based on the geobarometric equations (after Schmidt, 1992), pressure conditions estimated for granite gneiss and migmatites in the Suhum Basin range from 5.2 kbar to 7.2 kbar (Supplementary Table S7). Although pressure values are similar, the difference in the P-T range (~2 kbars) suggests that amphiboles underwent initial crystallisation at deeper depths, followed by a rather high magma ascension rate before final crystallisation (Ferreira et al., 2011). Conversely, the samples

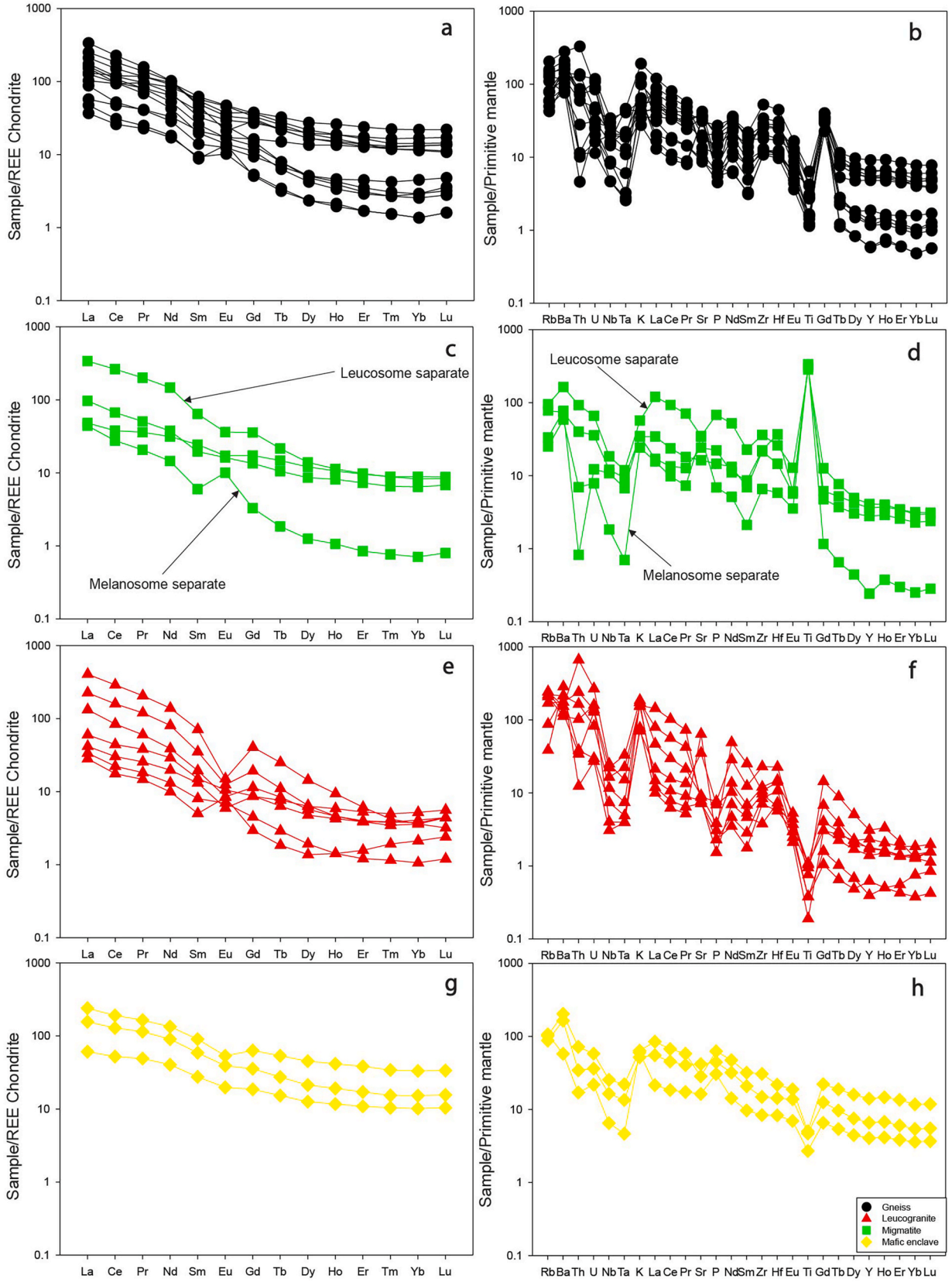

Fig. 10. Chondrite-normalised REE and primitive mantle-normalised diagrams of granite gneiss **(a) and (b)** Migmatites **(c) and (d)** leucogranites **(e) and (f)** mafic enclaves **(g) and (h)**. Chondrite and primitive normalizing values from Palme and O'Neill (2014).

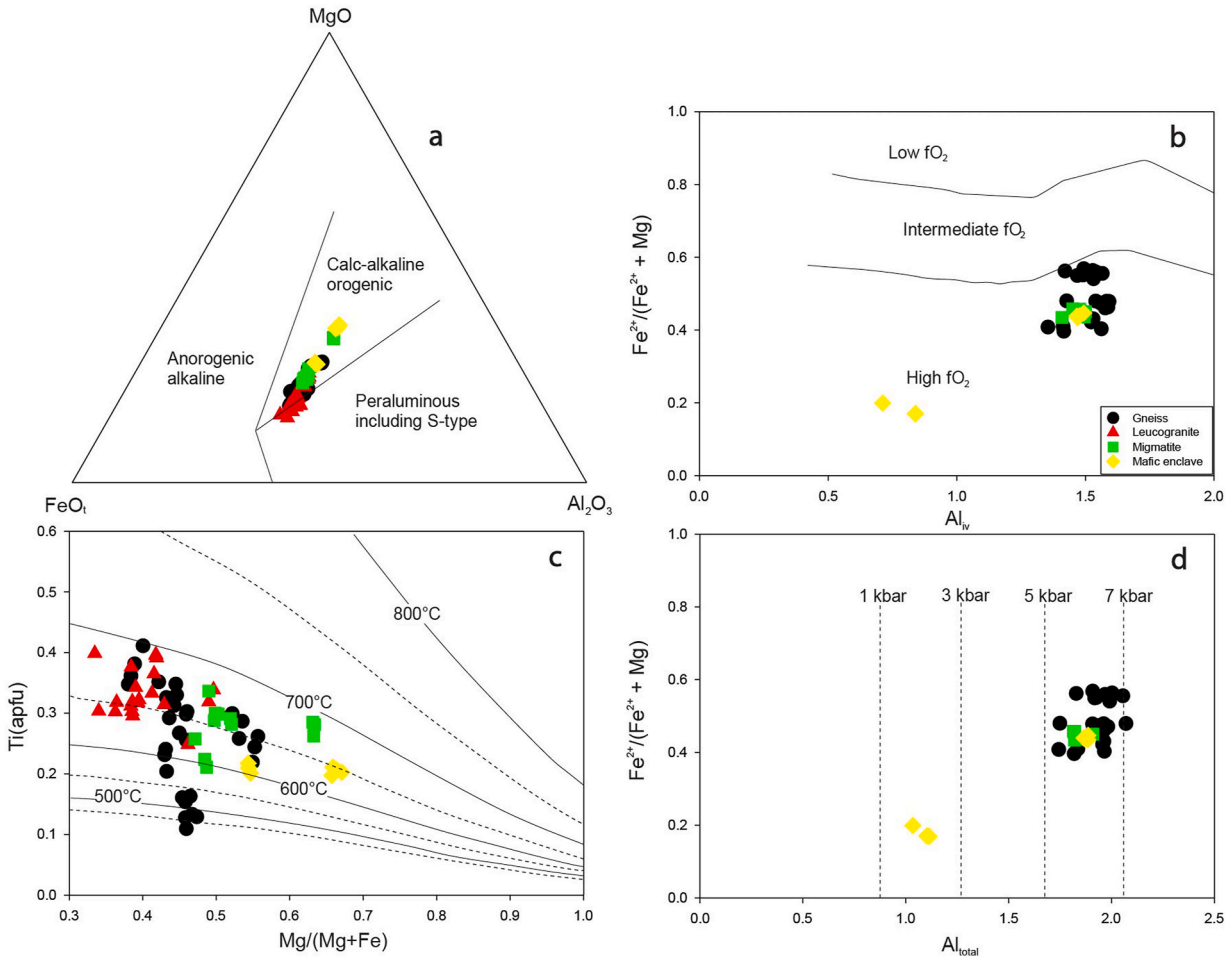

Fig. 11. **(a)** Tectonomagmatic discrimination diagram using FeO-MgO-Al_2O_3 of biotite from the granitoid complex of the Suhum Basin (Abdel-Rahman, 1994); **(b)** $Fe^{2+}/(Fe^{2+}+Mg)$ vs Al^{IV} diagram (after Anderson and Smith, 1995) showing the high fO2 nature of amphibole of the granitoid complex of the Suhum Basin; **(c)** Ti vs. $Mg/(Mg + Fe^{2+})$ diagram for the biotite (after Henry et al., 2005) showing formation temperatures; and **(d)** $Fe^{2+}/(Fe^{2+}+Mg)$ vs Al^{T} diagram (Schmidt, 1992).

plotted on the $Fe^{2+}/Fe^{2+}+Mg$ vs. Al (tot) diagram (Schmidt, 1992, Fig. 11d) fall within the pressure range of 5–7 kbar and further validate the calculated pressures. However, one mafic enclave sample has pressure calculations between 1.97 and 2.52 kbar and plots in the pressure range from 1 to 3 kbar (Fig. 11d). This anomalous P-T calculation obtained for this mafic enclave sample may be attributed to Al re-equilibration between coexisting amphibole and plagioclase during sub-solidus cooling (Ferreira et al., 2011; Tetsopgang et al., 2011).

The depth from which brittle deformation transitions to ductile deformation according to Wang et al. (2014) occurs approximately between the depths of 10–15 km. From the pressure estimates determined for the Suhum Basin granitoids (5.2–7.2 kbars) the depths of emplacement of the granitoids range from 19 to 27 km (based on the pressure distribution expression; 3.7 km/kbar = 37 km/GPa). This suggests that the granitoids are the products of partial melting and structural deformation of deep crustal material. Moreover, deformational features such as the penetrative foliation fabric, gneissic banding, medium-to coarse-grained texture, as well as shear and swirled structures associated with the granitoids (Figs. 3–5) present a historic record of deep (middle to lower) crustal level emplacement and deformation (Opare-Addo et al., 1993).

5. Discussion

5.1. Nature, redox state, and source of granitoid magma

The $Fe_t/(Fe_t + Mg)$ against total Al plot after Shabani et al. (2003) indicates that the studied biotite samples are Fe-rich biotite, plotting dominantly in the region on annite-siderophyllite (Fig. 6b). On Fig. 6b, the migmatites biotite has a composition akin to I-type granites. However, the granitic gneiss and leucogranite biotites show compositions comparable to strongly contaminated and reduced I-type granite, and I-type granite. From the whole-rock major element compositions, the granitoids samples fall entirely in the metaluminous field, which is a typical feature of I-type granitoids (Fig. 9a). Generally, I-type granitoids are derived in oxidised conditions as compared to S-type granitoids. This is because, I-type granitoids usually have higher ratios of Fe^{3+}/Fe^{2+}, which favours the formation of hornblende, biotite, and magnetite (Clemens & Stevens, 2012). Thus, the I-type signature coupled with the annite-siderophyllite composition of the studied biotite may indicate crystallisation of the granitoid complex of the Suhum Basin under oxidised conditions. High fO_2 suggests an oxidising condition during crystallisation of granitic magmas, which is the case for the rocks of the Suhum Basin (Fig. 11b).

The studied biotite samples from the granitoid complex of the Suhum Basin have FeO_t, Al_2O_3, and MgO compositions similar to those of calc-alkaline orogenic magmas, with the exception of some migmatite samples, which straddles the boundary line between calc-alkaline and peraluminous magmas (Fig. 11a). The calc-alkaline nature of the magma can also be inferred from the whole-rock major element compositions, where the samples fall in the calc-alkaline field on the AFM diagram (Fig. 9d). These geochemical features may connote that the granitoids were derived from the partial melting of older hydrous meta-igneous rocks (Roberts and Clemens, 1993). The medium-to-high-K character

of the rocks, coupled with their calc-alkaline nature, may be a reflection of the generation of the magma in regions where the mantle wedge might have interacted with enriched fluids from the underlying plate during dehydration (Roberts and Clemens, 1993). In many cases, fractional crystallisation via melting of the mantle has been proposed for calc-alkaline I-type granitoids. The generally enriched LREE with nearly flat to depleted HREE patterns depicted by the rocks of the Suhum Basin suggest derivation from enriched sources or a reflection of a high degree of fractional crystallisation (Fig. 10a, c, 10e, and 10g). The variably negative and positive Eu* shown by the Suhum Basin granitoids may also indicate partial melting from mixed sources, i.e., crust and mantle.

5.2. Record of magmatism and metamorphism

From the photomicrographs in Figs. 3 and 4, hornblende and plagioclase co-exist in the granitoids in the Suhum Basin. Based on the co-existence of these two minerals and the calc-alkaline nature of the rocks, we use the amphibole-plagioclase thermometric approach to estimate the temperature for the emplacement of the granitoids in the Suhum Basin. The co-existence of hornblende and plagioclase in calc-alkaline igneous terranes has been used by various workers (e.g., Holland and Blundy, 1994; Stein and Dietl, 2001), as a thermometric tool to estimate temperatures for their emplacement. According to Stein and Dietl (2001) although the use of this thermometric calibration is still under debate, there is no other known geothermometer that can be applied to calc-alkaline igneous rocks as of now. Blundy and Holland (1990) and Holland and Blundy (1994) approximated a symmetric formalisation that provides an appropriate framework and equations to formulate amphibolite-plagioclase thermometers. The reaction calibration is stated in the equations below.

(a) Edenite + 4 quartz = albite + tremolite
(b) Albite + edemite = richterite + anorthite.

This study is able to use this equation, and the empirical thermometer based on the edenite-tremolite reaction by Blundy and Holland (1990) and Holland and Blundy (1994) because the plagioclase of the Suhum Basin granitoids has a less than 0.90 atoms p.f.u. and Si in hornblende is less than 7.8 atoms p.f. u. (Supplementary Tables S2 and S4). These values are acceptable to calibrate well for temperatures ranging from 500 °C to 1100 °C. From the rocks analysed in the Suhum Basin, the granite gneiss was crystallised between 632 °C and 712 °C. The occurrence and coexistence of plagioclase (oligoclase to andesine) and amphibole, which are common in the Suhum Basin granitoids, constitute the most common mineral assemblages found in rocks formed at amphibolite facies conditions (Spear, 1993). A progressive retrograde path towards greenschist facies conditions can be explained by the occurrence of epidote and chlorite as secondary alteration phases. The greenschist and amphibolite facies metamorphic grades described for the Birimian terrane represent the widespread and most common facies of metamorphism under which mountain building occurs (DiPietro, 2013).

To place the P-T conditions of the Suhum Basin in the context of the Birimian terrane in Ghana, P-T data derived from volcanic successions and granitoid domains suggest that regional P-T conditions were clockwise and reached amphibolite facies during the Eburnean orogeny and later retrograded to greenschist facies conditions (John et al., 1999; Doumbia et al., 1998; Feybesse et al., 2006; Grenholm, 2011). Klemd et al. (2002) reported peak P-T conditions of 500–610 °C and 4.5–6 kbar for metapelites and amphibolites in the southern Kibi-Winneba belt. Conventional geothermobarometry and P-T phase modelling data from the southern Ashanti belt by John et al. (1999) and White et al. (2013) yielded peak conditions of 500–650 °C at 5–6 kbar and 595 °C at 5 kbar, respectively. Similar P-T conditions have also been reported by Galipp et al. (2003) in the central parts of the Sefwi volcanic belt. Opare-Addo et al. (1993) reported P-T conditions at 600–1000 °C at 5–8.5 kbar for the migmatites exposed within the Suhum domain. This means, the estimated P-T conditions (600–700 °C at 5.2–7.2 kbar) for the Suhum Basin granitoids in this study are in the range of those reported for other Birimian terrane in Ghana. In this study, the relatively high-pressure conditions of emplacement probably took place in an arc-type setting (convergent margin) during the collisional and post-collisional tectonic phase associated with possible crustal thickening in addition to the vertical uplift and erosion (Tetsopgang et al., 2011).

The rocks of the Suhum Basin regularly contain amphiboles but bear no distinctive peraluminous minerals like garnet or cordierite, except the leucogranites, which have biotite as the only mafic mineral. S-type granitoids contain aluminium-rich bearing phases (e.g., cordierite, sillimanite, muscovite, e. t.c), while I-type granitoids are metaluminous and are mostly amphibole-bearing (Frost et al., 2001; Chappell et al., 2012). These mineralogical features strongly imply that the studied rocks possess I-type characteristics. The rocks from the Suhum Basin also have A/CNK values typical of metaluminous I-type granitoids. This may suggest that they are products of partial melting of a mafic mantle-derived igneous source material (probably of a sub-crustal underplate, but subducted-slab crust or older high-level pluton sources cannot be excluded) (Barbarin, 1990; 1999). Calc-alkaline granitoids, are mostly characterised by K enrichment, which is dominant in deep crustal material (Rudnick and Taylor, 1987; Wang et al., 2014). The granitoids of the Suhum Basin possess high-K calc-alkaline characteristics and metaluminous signatures, which hint towards their origination from deeper crustal levels (Wang et al., 2014). Their biotite composition suggests derivation from mixed crustal and mantle sources (Fig. 12a; Zhou, 1986). This assertion, together with the field observation of abundant mafic restitic enclaves in the granite gneiss, argues in favour of their origin from partial melting of a mafic igneous precursor (Frost et al., 2001). The occurrence of biotite-hornblende and biotite-bearing granitic rocks within the Suhum Basin, and the absence of two-mica granitoids also rule out sediment contribution in the Suhum Basin (Grenholm, 2011).

The trace element characteristics of the Suhum Basin rocks are akin to those of I-type rocks, and thus can be interpreted as derivatives from a mafic igneous precursor (thickened mafic lower crust), generated in convergent margins (Liu et al., 2019; Sakyi et al., 2020a). This is supported by the occurrence of mafic layers within the granitoids. On the other hand, the trace element patterns presented in this study may also suggest that the parental magmas of the granitoids were generated through the partial melting of a hot, subducting slab in a subduction related island-arc environment (Defant and Drummond, 1990; Drummond et al., 1996; Smithies, 2000). The Ti, Nb, and Ta negative peaks on the primitive-mantle normalised multi-element plot (Fig. 10), alongside weak positive Zr-Hf anomalies, indicative of continental crust origin (Elburg, 2010; Rudnick and Gao, 2003). The variably negative and positive Eu* shown by the Suhum Basin granitoids may also indicate partial melting from mixed sources, i.e., crust and mantle. Moreover, the granitoids exhibit low Sr/Y ratios, with high Yb (>1.0 ppm) and Y (>10 ppm) contents, further suggesting that their formation involved the melting of crustal material.

Trace element characteristics of the leucogranites, such as enrichment in LREE, LILE (Rb and K) and depletion in HFSE (Nb, Ta, and Ti), signal the involvement of crustal sources (Liu et al., 2019). Their higher Sr (75.6–1405.8 ppm) but lower Y (1.63–12.77 ppm) and Yb (0.18–0.88 ppm) contents lead to very high Sr/Y ratios of 15.58–549.14. Although all samples share a broadly coherent trace element signature, the diversity of the leucogranites indicates variable degrees of partial melting and/or fractional crystallisation of the parent melt in their petrogenesis. The $(La/Yb)_N$ ratios (7.71–108.04) of the leucogranites also suggest they were derived from crustal melt which is affirmed by their field occurrence as intrusive bodies generated probably by small melt volumes rather than large plutonic masses.

Generally, I-type leucogranites are usually associated with mixed magma sources or mantle-derived tholeiitic magma formed within arc-

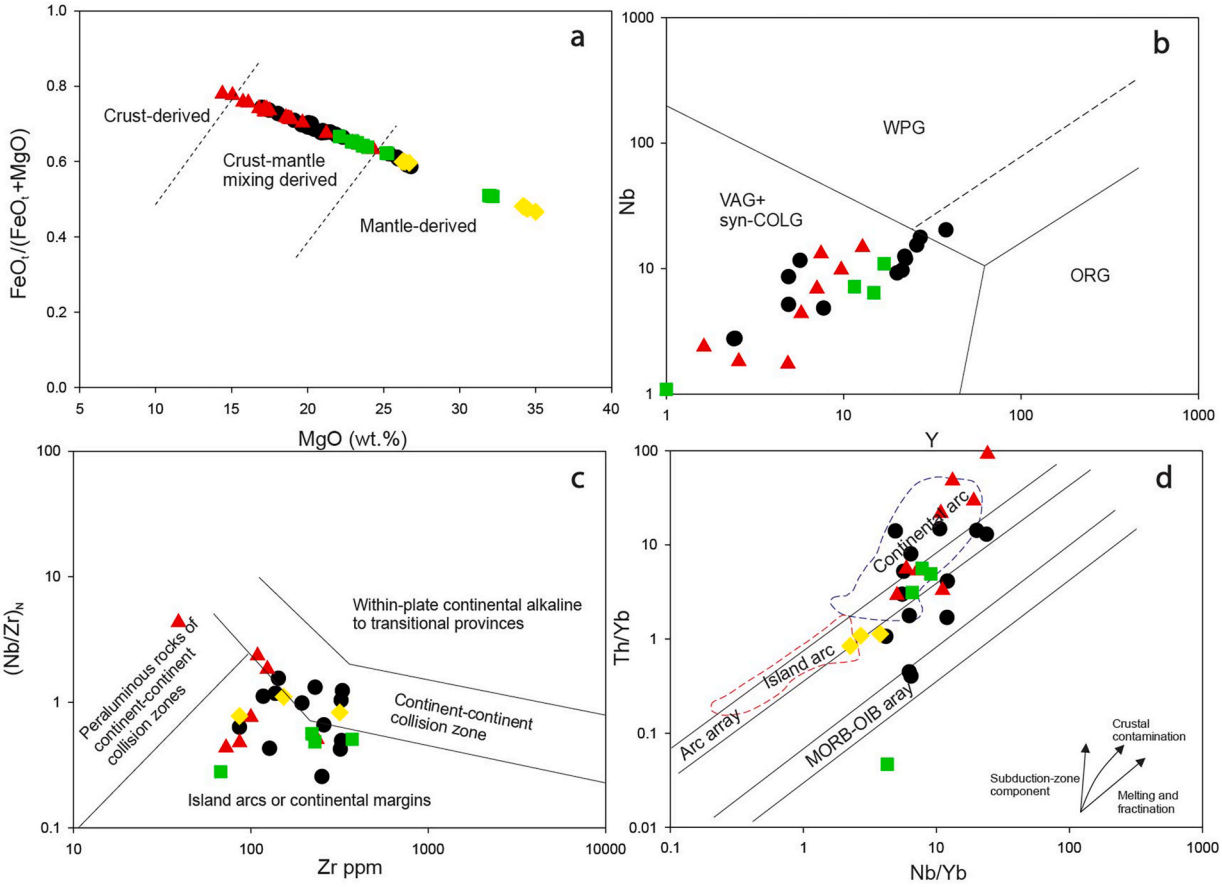

Fig. 12. Tectonic discriminant diagrams for the granitoid complex of the Suhum Basin **(a)** Mg vs. Fe/Fe + Mg; **(b)** Nb vs. Y after Pearce et al. (1984); **(C)** Zr vs. $(Nb/Zr)_N$ diagram of Thieblemont and Tegyey (1994); and **(d)** Th/Yb vs. Nb/Yb with reference fields modified after Pearce. (2008).

type settings, including volcanic arcs and late or post-collision settings (Athari et al., 2008). Most studied leucogranites exposed within the Birimian terrane are interpreted as products of shallow partial melting of older enriched crustal sources in a thickened crust during the Eburnean tectonothermal orogeny (e.g., Doumbia et al., 1998; Feybesse et al., 2006; Grenholm, 2011; Petersson et al., 2016; McFarlane et al., 2019). Lateral equivalents of Birimian leucogranites exposed in French Guyana have been described as the products of crustal thickening and anatexis along major shear zones resulting from oblique collision and late orogenic lateral extrusion (Kroonenberg et al., 2016).

5.3. Implications for tectonic setting

Based on petrography and mineral chemistry, green to greenish brown biotite observed in the various rock types and known to be Mg- and Fe-rich is typical of arc-related suites (Lalonde and Bernard, 1993). These biotite varieties are mostly moderately oxidised and are typical of the more voluminous magmatism of continental arcs. The abundance of hydrated minerals (e.g., biotite and amphibole) in plutonic rocks suggests that the melting of their protolith took place under hydrous conditions. The abundance of calcic amphiboles determined from mineral chemistry points to the I-type nature of the Suhum Basin granitoids, which were emplaced in a subduction environment in relation to an active continental margin (e.g., Chappell et al., 2012; Sakyi et al., 2014; Esfahani et al., 2017; Sakyi et al., 2020a). The calc-alkaline nature of the studied rocks is largely constrained by subduction-related processes and thus can be attributed to an arc-type environment.

Trace element concentrations are somewhat related to volcanic-arc maturity, e.g., granitoids originating from continental arcs with calc-alkaline affinities usually possess decoupled LILE and LREE enrichments with depleted HREE and HFSE content and low HFSE/LILE ratios (e.g., Sakyi et al., 2014; Wang et al., 2014; Sakyi et al., 2020a). Primitive mantle-normalised spider diagrams (Fig. 10b, d, 10f, and 10h) for the studied rocks are characteristic of rocks derived from subduction zones (Harris et al., 1986). In addition, the high LILE and LREE contents also suggest the impact of subduction-related components during the melting process in an arc-type setting (Anum et al., 2015). All these signatures further support the argument that the studied rocks originated from arc or collisional settings preceded by a period of crustal thickening (Liu et al., 2019; Sakyi et al., 2020a).

In the trace element discriminant diagrams (Pearce et al., 1984), the studied rocks plot mainly within the volcanic arc and syn-collisional granitoid array (Fig. 12b). On the Zr vs. Nb/Zr diagram, the studied rocks from the Suhum Basin plot dominantly in the island-arc or continental margin field, with a few samples, mostly granite gneiss plotting the continent-continent collision zone (Fig. 12c). The studied rocks define a linear trend mainly within the continental arc array in the tectonic setting discrimination diagram after Pearce (2008) (Fig. 12d). All these further constraints their subduction related origin.

5.4. Implications for the evolution of the Birimian granitoids in the West African Craton (WAC)

The regional geodynamic model for the evolution of the Paleoproterozoic Birimian terrane of the Southern West African Craton (sWAC) has been subjected to several controversies. Diverse models have been proposed by different schools of thought to explain the geodynamic evolution of the Birimian terrane of the West African Craton (WAC). Regional geochemical dataset compilation by Grenholm et al. (2019) illustrates that the Birimian intrusives across the sWAC are

predominantly calc-alkaline, metaluminous to mildly peraluminous, and magnesian to weakly ferroan. The trace element signatures of magmatic suites that comprise the Birimian terrane exhibit ubiquitous negative Nb-Ta troughs, negative P and Ti anomalies coupled with positive Pb anomalies, and variable LILE enrichment and HFSE depletion.

The signatures exhibited by the Suhum Basin granitoids do not differ significantly from other granitoid domains within the Birimian terrane with respect to their petrological and geochemical characteristics (e.g., de Kock et al., 2011; Sakyi et al., 2014; Anum et al., 2015; Block et al., 2016b; McFarlane et al., 2019; Parra-Avila et al., 2019). All the samples analysed in this study are also consistent with the trace element patterns of the present-day bulk continental crust composition (Rudnick and Gao, 2003; Hawkesworth and Kemp, 2006). Such features typify arc magmas and crust formation in a subduction setting and are therefore consistent with the onset of "modern-style" subduction-related processes after 3.0 Ga (Dampare et al., 2008; Sakyi et al., 2014; Anum et al., 2015; Block et al., 2016b; McFarlane et al., 2019).

6. Conclusions

Petrographic, geochemical, and mineral chemistry data of the granitoid complex of the Paleoproterozoic Suhum Basin of southern Ghana have been presented in this study. The rocks are broadly categorized into granite gneiss (amphibole-bearing gneiss and biotite gneiss), migmatites, intrusive leucogranites, and mafic enclaves. These rocks possess calc-alkaline, I-type, metaluminous to weakly peraluminous characteristics and are subduction-zone related. They were formed during a single orogenic event in a continental arc setting where subduction zone components played a role in the generation of their parental magmas. Thermobarometric calculations using amphibole and plagioclase, yield P-T estimates of ~600–712 °C and pressures ranging between 5.2 and 7.2 kbar. The pressures calculated for the granitoid complex exceed the depth of transition from brittle to ductile style of deformation (10–15 km), thus implying that they originated from deeper crustal levels (19–27 km).

CRediT authorship contribution statement

Daniel Kwayisi: Writing – review & editing, Writing – original draft, Software, Investigation, Data curation, Conceptualization. **Prince Ofori Amponsah:** Writing – review & editing, Writing – original draft, Supervision, Investigation, Data curation, Conceptualization. **Emmanuel Kwaku Awunyo:** Writing – review & editing, Writing – original draft. **Marian Selorm Sapah:** Writing – review & editing, Writing – original draft, Supervision. **Patrick Asamoah Sakyi:** Writing – review & editing, Writing – original draft, Methodology, Conceptualization. **Ben-Xun Su:** Writing – review & editing, Writing – original draft, Methodology, Formal analysis. **Prosper M. Nude:** Writing – review & editing, Writing – original draft. **Abigail Enyonam Ayikwei:** Writing – review & editing, Writing – original draft, Supervision. **Eric Dominic Forson:** Writing – review & editing, Writing – original draft, Data curation.

Declaration of competing interest

The authors declare the following financial interests/personal relationships which may be considered as potential competing interests: Nothing of the sort If there are other authors, they declare that they have no known competing financial interests or personal relationships that could have appeared to influence the work reported in this paper.

Acknowledgement

The authors are grateful to the entire personnel of the State Key Laboratory of Lithospheric Evolution and the Key Laboratory of Mineral Resources, Institute of Geology and Geophysics, Chinese Academy of Sciences, for their diverse roles in all of the analyses. The authors would like to thank the editor and the two anonymous reviewers for taking their time to review the manuscript.

Appendix A. Supplementary data

Supplementary data to this article can be found online at https://doi.org/10.1016/j.jafrearsci.2024.105475.

Data availability

Data will be made available on request.

References

Abdel-Rahman, A.F.M., 1994. Nature of biotites from alkaline, calc-alkaline, and peraluminous magmas. J. Petrol. 35 (2), 525–541.
Abitty, E.K., Dampare, S.B., Nude, P.M., Asiedu, D.K., 2016. Geochemistry and petrogenesis of the K-rich 'bongo-type'granitoids in the paleoproterozoic bole–nangodi greenstone belt of Ghana. J. Afr. Earth Sci. 122, 47–62.
Abouchami, W., Boher, M., Michard, A., Albarede, F., 1990. A major 2.1 Ga event of mafic magmatism in West Africa: an early stage of crustal accretion. J. Geophys. Res. Solid Earth 95 (B11), 17605–17629.
Adams, S.J., Van Lichtervelde, M., Amponsah, P.O., Nude, P.M., Asiedu, D.K., Dampare, S.B., 2023. Characterisation and rare-metal potential of the Winneba-Mankoadze pegmatites, Southern Ghana: evidence of two pegmatite fields. J. Afr. Earth Sci. 207, 105049.
Agra, N.A., Elburg, M.A., Vorster, C., 2023. Constraints on paleoproterozoic crustal growth from birimian supergroup lavas of the Bui belt (Ghana) in the West african craton. Precambrian Res. 384, 106926.
Agyei Duodu, J., Loh, G.K., Hirdes, W., Boamah, K.O., Baba, M., Anokwa, Y.M., Asare, C., Brako-hiapa, E., Mensah, R.B., Okla, R., Toloczyki, M., Davis, D.W., Glück, S., 2009. Geological Map of Ghana 1:1 000 000. BGS/GGS, Accra, Ghana/Hannover,Germany.
Amponsah, P.O., Salvi, S., Didier, B., Baratoux, L., Siebenaller, L., Jessell, M., Nude, P.M., Gyawu, E.A., 2016a. Multistage gold mineralization in the Wa-Lawra greenstone belt, NW Ghana: the Bepkong deposit. J. Afr. Earth Sci. 120, 220–237.
Amponsah, P.O., Salvi, S., Béziat, D., Baratoux, L., Siebenaller, L., Nude, P.M., Nyarko, R. S., Jessell, M.W., 2016b. The Bepkong gold deposit, northwestern Ghana. Ore Geol. Rev. 78, 718–723.
Amponsah, P.O., Kwayisi, D., Awunyo, E.K., Sapah, M.S., Sakyi, P.A., Su, B.-X., Lu, Y., Nude, P.M., 2023. New evidence for crustal reworking and juvenile arc-magmatism during the Palaeoproterozoic Eburnean events in the Suhum Basin, South-east Ghana. Geol. J. https://doi.org/10.1002/gj.4790.
Amponsah, P.O., Forson, E.D., 2023. Geospatial modelling of mineral potential zones using data-driven based weighting factor and statistical index techniques. J. Afr. Earth Sci. 206, 105020.
Amponsah, P.O., Forson, E.D., 2024. Mineral prospectivity modeling over julie tenement of northwestern Ghana using geophysical datasets. J. Mining and Environ. 15 (3), 791–816.
Andersson, U.B., Begg, G.C., Griffin, W.L., Högdahl, K., 2011. Ancient and juvenile components in the continental crust and mantle: Hf isotopes in zircon from Svecofennian magmatic rocks and rapakivi granites in Sweden. Lithosphere 3 (6), 409–419.
Anderson, J.L., Smith, D.R., 1995. The effects of temperature and fO2 on the Al-in-hornblende barometer. Am. Mineral. 80 (5–6), 549–559.
Anum, S., Sakyi, P.A., Su, B.X., Nude, P.M., Nyame, F., Asiedu, D., Kwayisi, D., 2015. Geochemistry and geochronology of granitoids in the Kibi-Asamankese area of the Kibi-Winneba volcanic belt, southern Ghana. J. Afr. Earth Sci. 102, 166–179.
Asiedu, D.K., Agoe, M., Amponsah, P.O., Nude, P.M., Anani, C.Y., 2019. Geochemical constraints on provenance and source area weathering of metasedimentary rocks from the Paleoproterozoic (~ 2.1 Ga) Wa-Lawra Belt, southeastern margin of the West African Craton. Geodin. Acta 31 (1), 27–39.
Atanga, F., Amponsah, P.O., Nunoo, S., Kwayisi, D., Forson, E.D., Akabzaa, T.M., Nude, P.M., 2023. The geology and geochemistry of the Rhyacian Josephine gold deposit, Northwest Ghana. B. Appl. Earth Sci. 132 (3–4), 252–270.
Athari, S.F., Sepahi, A.A., Moazzen, M., 2008. Petrology of leucocratic granitoids in the northwest of Iran with emphasis on leucocratic I-type granites from SW Saqqez. Neues Jahrbuch Mineral. Abhand. 184 (2), 169–179. https://doi.org/10.1127/0077-7757/2007/0088.
Baratoux, L., Metelka, V., Naba, S., Jessell, M.W., Grégoire, M., Ganne, J., 2011. Juvenile Paleoproterozoic crust evolution during the Eburnean orogeny (~ 2.2–2.0 Ga), western Burkina Faso. Precambrian Res. 191 (1–2), 18–45.
Barbarin, B., 1990. Granitoids: main petrogenetic classifications in relation to origin and tectonic setting. Geol. J. 25 (3–4), 227–238. https://doi.org/10.1002/gj.3350250306.
Barbarin, B., 1999. A review of the relationships between granitoid types, their origins and their geodynamic environments. Lithos 46 (3), 605–626. https://doi.org/10.1016/S0024-4937(98)00085-1.
Block, S., Baratoux, L., Zeh, A., Laurent, O., Bruguier, O., Jessell, M., Ailleres, L., Sagna, R., Parra-Avila, L., Bosch, D., 2016b. Paleoproterozoic juvenile crust formation and stabilisation in the south-eastern West African Craton (Ghana); New

insights from U-Pb-Hf zircon data and geochemistry. Precambrian Res. 287, 1–30. https://doi.org/10.1016/j.precamres.2016.10.011.
Block, S., Jessell, M., Aillères, L., Baratoux, L., Bruguier, O., Zeh, A., Bosch, D., Caby, R., Mensah, E., 2016a. Lower crust exhumation during Paleoproterozoic (Eburnean) orogeny, NW Ghana, West African Craton: interplay of coeval contractional deformation and extensional gravitational collapse. Precambrian Res. 274, 82–109. https://doi.org/10.1016/j.precamres.2015.10.014.
Blundy, J.D., Holland, T.J.B., 1990. Calcic amphibole equilibria and a new amphibole-plagioclase geothermometer. Contirbutions to Mineral. Petrol. 104, 208–224.
Bucher, K., Frey, M., 2002. Petrogenesis of metamorphic rocks. Springer Sci. & Bus. Media.
Bonhomme, M., 1962. Contribution a' l'étude géochronologique de la plate-forme de l'Ouest africain. Ann. Fac. Sci. Univ. Clermont-Ferrand 5.
Clemens, J.D., Stevens, G., 2012. What controls chemical variation in granitic magmas? Lithos 134–135, 317–329.
Chappell, B.W., Bryant, C.J., Wyborn, D., 2012. Peraluminous I-type granites. Lithos 153, 142–153.
Chu, Z.Y., Wu, F.Y., Walker, R.J., Rudnick, R.L., Pitcher, L., Puchtel, I.S., Yang, Y.H., Wilde, S.A., 2009. Temporal evolution of the lithospheric mantle beneath the eastern North China Craton. J. Petrol. 50 (10), 1857–1898.
Condie, K.C., 1998. Episodic continental growth and supercontinents: a mantle avalanche connection? Earth Planet Sci. Lett. 163 (1–4), 97–108. https://doi.org/10.1016/S0012-821X(98)00178-2.
Condie, K.C., O'Neill, C., Aster, R.C., 2009. Evidence and implications for a widespread magmatic shutdown for 250 My on Earth. Earth Planet Sci. Lett. 282 (1–4), 294–298. https://doi.org/10.1016/J.EPSL.2009.03.033.
Dampare, S.B., Shibata, T., Asiedu, D.K., Osae, S., Banoeng-Yakubo, B., 2008. Geochemistry of Paleoproterozoic metavolcanic rocks from the southern Ashanti volcanic belt, Ghana: petrogenetic and tectonic setting implications. Precambrian Res. 162 (3–4), 403–423.
Defant, M.J., Drummond, M.S., 1990. Derivation of some modern arc magmas by melting of young, subducted lithosphere. Nature 347 (6294), 662–665.
de Kock, G.S., Armstrong, R.A., Siegfried, H.P., Thomas, E., 2011. Geochronology of the birim supergroup of the West african craton in the wa-bolé region of west-central Ghana: implications for the stratigraphic framework. J. Afr. Earth Sci. 59 (1), 1–40.
Diatta, F., Ndiaye, P.M., Diène, M., Amponsah, P.O., Ganne, J., 2017. The structural evolution of the Dialé-Daléma basin, Kédougou-Kéniéba Inlier, eastern Senegal. J. Afr. Earth Sci. 129, 923–933.
DiPietro, J.A., 2013. Keys to the Interpretation of Geological History. *Landscape Evolution in the United States*, pp. 327–344.
Doumbia, S., Pouclet, A., Kouamelan, A., Peucat, J.J., Vidal, M., Delor, C., 1998. Petrogenesis of juvenile-type birimian (paleoproterozoic) granitoids in central côte-d'Ivoire, West Africa: geochemistry and geochronology. Precambrian Res. 87 (1–2), 33–63. https://doi.org/10.1016/S0301-9268(97)00201-5.
Drummond, M.S., Defant, M.J., Kepezhinskas, P.K., 1996. Petrogenesis of slab-derived trondhjemite–tonalite–dacite/adakite magmas. Earth and Environ. Sci. Transact. Royal Soc. Edinburgh 87 (1–2), 205–215.
Elburg, M.A., 2010. Sources and processes in arc magmatism: The crucial role of water (An inaugural lecture to the Society). Geol. Belg.
Esfahani, M.M., Khalili, M., Bakhshi, M., 2017. Petrogenesis of Soheyle-Pakuh and Golshekanan granitoid based on mineral chemistry of ferromagnesian minerals (north of Nain), Iran. J. Afr. Earth Sci. 129, 973–986.
Feng, X., Wang, E., Amponsah, P.O., Ganne, J., Martin, R., Jessell, M.W., 2019. Effect of pre-existing faults on the distribution of lower crust exhumation under extension: numerical modelling and implications for NW Ghana. Geosci. J. 23, 961–975.
Feng, X., Wang, E., Ganne, J., Amponsah, P., Martin, R., 2018. Role of volcano-sedimentary basins in the formation of greenstone-granitoid belts in the West African craton: a numerical model. Minerals 8 (2), 73.
Ferreira, V.P., Sial, A.N., Pimentel, M.M., Armstrong, R., Spicuzza, M.J., Guimarães, I.P., da Silva Filho, A.F., 2011. Contrasting sources and P-T crystallization conditions of epidote-bearing granitic rocks, northeastern Brazil: O, Sr, and Nd isotopes. Lithos 121 (1–4), 189–201. https://doi.org/10.1016/j.lithos.2010.11.002.
Feybesse, J., Billa, M., Guerrot, C., Duguey, E., Lescuyer, J., Milesi, J., Bouchot, V., 2006. The paleoproterozoic Ghanaian province: geodynamic model and ore controls, including regional stress modeling, 149–196. https://doi.org/10.1016/j.precamres.2006.06.003.
Forson, E.D., Amponsah, P.O., Hagan, G.B., Sapah, M.S., 2023. Frequency ratio-based flood vulnerability modeling over the greater Accra Region of Ghana. Modeling Earth Systems and Environ. 9 (2), 2081–2100.
Forson, E.D., Amponsah, P.O., Wemegah, D.D., Ahwireng, M.D., 2024. Random forest-based mineral prospectivity modelling over the Southern Kibi–Winneba belt of Ghana using geophysical and remote sensing techniques. B. Appl. Earth Sci., 25726838231225055
Forson, E.D., Menyeh, A., Wemegah, D.D., 2021. Mapping lithological units, structural lineaments and alteration zones in the Southern Kibi- Winneba Belt of Ghana using integrated geophysical and remote sensing datasets. Ore Geol. Rev. 137, 104271.
Forson, E.D., Amponsah, P.O., 2023. Prediction of gold mineralization zones using spatial techniques and geophysical data: a case study of the Josephine prospecting licence, NW Ghana. Heliyon 9 (11), e22398.
Frost, B.R., Frost, C.D., 2008. A geochemical classification for feldspathic igneous rocks. J. Petrol. 49 (11), 1955–1969.
Frost, B.R., Barnes, C.G., Collins, W.J., Arculus, R.J., Ellis, D.J., Frost, C.D., 2001. A geochemical classification for granitic rocks. J. Petrol. 42 (11), 2033–2048. https://doi.org/10.1093/petrology/42.11.2033.
Galipp, K., Klemd, R., Hirdes, W., 2003. Metamorphism and geochemistry of the paleoproterozoic Birimian sefwi volcanic belt (Ghana, West Africa). Geol. Jahrb. D 111, 151–191.
Gastil, R.G., 1960. The distribution of mineral dates in time and space. Am. J. Sci. 258 (1), 1–35.
Gasquet, D., Barbey, P., Adou, M., Paquette, J.L., 2003. Structure, Sr–Nd isotope geochemistry and zircon U–Pb geochronology of the granitoids of the Dabakala area (Côte d'Ivoire): evidence for a 2.3 Ga crustal growth event in the Palaeoproterozoic of West Africa? Precambrian Res. 127 (4), 329–354.
Giret, A., Bonin, B., Leger, J.M., 1980. Amphibole compositional trends in oversaturated and undersaturated alkaline plutonic ring-composition. Can. Mineral. 18 (4), 481–495.
Gong, S., He, C., Wang, X.C., Chen, N., Kusky, T., 2019. No plate tectonic shutdown in the early Paleoproterozoic: constraints from the ca. 2.4 Ga granitoids in the Quanji Massif, NW China. J. Asian Earth Sci. 172, 221–242.
Grenholm, M., 2011. Petrology of Birimian granites in southern Ghana – petrography and petrogenesis. Sciences 285 (285).
Grenholm, M., Jessell, M., Thébaud, N., 2019. A geodynamic model for the Paleoproterozoic (ca. 2.27–1.96 Ga) Birimian Orogen of the southern West African Craton – insights into an evolving accretionary-collisional orogenic system. Earth Sci. Rev. 192 (July 2018), 138–193. https://doi.org/10.1016/j.earscirev.2019.02.006.
Hammarstrom, J.M., Zen, E.A., 1986. Aluminum in hornblende: an empirical igneous geobarometer. Am. Mineral. 71 (11–12), 1297–1313.
Harris, N.B., Pearce, J.A., Tindle, A.G., 1986. Geochemical characteristics of collision-zone magmatism. Geological Society 19 (1), 67–81.
Hawkesworth, C.J., Dhuime, B., Pietranik, A.B., Cawood, P.A., Kemp, A.I., Storey, C.D., 2010. The generation and evolution of the continental crust. J. Geol. Soc. 167 (2), 229–248.
Hawkesworth, C.J., Kemp, A.I.S., 2006. Evolution of the continental crust. Nature 443 (7113), 811–817.
Henry, D.J., Guidotti, C.V., Thomson, J.A., 2005. The Ti-saturation surface for low-to-medium pressure metapelitic biotites: implications for geothermometry and Ti-substitution mechanisms. Am. Mineral. 90 (2–3), 316–328.
Hirdes, W., Davis, D.W., Eisenlohr, B.N., 1992. Reassessment of Proterozoic granitoid ages in Ghana on the basis of U/Pb zircon and monazite dating. Precambrian Res. 56 (1–2), 89–96.
Holland, T., Blundy, J., 1994. Non-ideal interactions in calcic amphiboles and their bearing on amphibole-plagioclase thermometry. Contrib. Mineral. Petrol. 116, 433–447.
Hollister, L.S., Grissom, G.C., Peters, E.K., Stowell, H.H., Sisson, V.B., 1987. Confirmation of the empirical correlation of Al in hornblende with pressure of solidification of calc-alkaline plutons. Am. Mineral. 72 (3–4), 231–239.
Howie, R.A., Zussman, J., Deer, W., 1992. An Introduction to the Rock-Forming Minerals. Longman, London, UK, p. 696.
Irvine, T.N., Baragar, W.R.A., 1971. A guide to the chemical classification of the common volcanic rocks. Can. J. Earth Sci. 8 (5), 523–548.
Jessell, M.W., Amponsah, P.O., Baratoux, L., Asiedu, D.K., Loh, G.K., Ganne, J., 2012. Crustal-scale transcurrent shearing in the paleoproterozoic sefwi-sunyani-comoe region, West Africa. Precambrian Res. 212, 155–168.
John, T., Klemd, R., Hirdes, W., Loh, G., 1999. The metamorphic evolution of the paleoproterozoic (birimian) volcanic Ashanti belt (Ghana, West Africa). Precambrian Res. 98 (1–2), 11–30. https://doi.org/10.1016/S0301-9268(99)00024-8.
Johnson, M.C., Rutherford, M.J., 1989. Experimental calibration of the aluminum-in-hornblende geobarometer with application to Long Valley caldera (California) volcanic rocks. Geology 17 (9), 837–841.
Kazapoe, R.W., Okunlola, O., Arhin, E., Olisa, O., Harris, C., Kwayisi, D., Torkorno, S., Amuah, E.E.Y., 2022. Geology and isotope systematics of gold deposits in the abansuoso area of the sefwi belt, southwestern Ghana. Geol., Ecol., and Landscapes 1–22.
Kazapoe, R.W., Okunlola, O., Arhin, E., Olisa, O., Kwayisi, D., Dzikunoo, E.A., Amuah, E.E.Y., 2023. Compositional characteristics of mineralised and unmineralised gneisses and schist around the Abansuoso area, southwestern Ghana. B. Appl. Earth Sci. 132 (1), 36–51.
Klemd, R., Hünken, U., Olesch, M., 2002. Metamorphism of the country rocks hosting gold–sulfide-bearing quartz veins in the Paleoproterozoic southern Kibi-Winneba belt (SE-Ghana). J. Afr. Earth Sci. 35 (2), 199–211.
Kouamelan, A.N., Djro, S.C., Allialy, M.E., Paquette, J.L., Peucat, J.J., 2015. The oldest rock of Ivory Coast. J. Afr. Earth Sci. 103, 65–70.
Kroonenberg, S.B., De Roever, E.W.F., Fraga, L.M., Reis, N.J., Faraco, T., Lafon, J.M., et al., 2016. Paleoproterozoic evolution of the Guiana Shield in Suriname: a revised model. Neth. J. Geosci. 95 (4), 491–522.
Lalonde, A.E., Bernard, P., 1993. Composition and color of biotite from granites; two useful properties in characterization of plutonic suites from the Hepburn internal zone of Wopmay Orogen, Northwest Territories. Can. Mineral. 31 (1), 203–217.
Leake, B.E., Wooley, A.R., Arps, C.E.S., Birch, W.D., Gilbert, M.C., Grice, J.D., Hawthorne, F.C., Kato, A., Kisch, H.J., Krivivichev, V.G., Linthout, K., Laird, J., Mandarino, J.A., Maresch, W.V., Nickel, E.H., Rock, N.M.S., Schumacher, J.C., Smith, D.C., Stephenson, N.C.N., Ungaretti, L., Whittaker, E.J.W., Youzhi, G., 1997. Nomenclature of amphiboles: report of the subcommittee on amphiboles of the International Mineralogical Asociation, commission on new minerals and mineral names. Am. Mineral. 82, 1019–1037.
Leube, A., Hirdes, W., Mauer, R., Kesse, G.O., 1990. The early Proterozoic Birimian Supergroup of Ghana and some aspects of its associated gold mineralization. Precambrian Res. 46 (1–2), 139–165.

Liu, X., Liu, W., Si, C., 2019. Petrogenesis and source rocks of the high-K calc-alkaline and shoshonitic I-type granitoids in the northwestern part of East Junggar, NW China. Lithos 326, 298–312.
Loh, G., Hirdes, W., Anani, C., Davis, D.W., Vetter, U.K., 1999. Explanatory Notes for the Geological Map of-Southwest Ghana 1:100,000-Sekondi (0402A) and Axim (0403B) Sheets. In: Geologisches Jahrbuch Reihe B Heft 93. BGR, Hannover.
Lompo, M., 2009. Geodynamic evolution of the 2.25-2.0 Ga Palaeoproterozoic magmatic rocks in the Man-Leo Shield of the West African Craton. A model of subsidence of an oceanic plateau. Geological Society 323 (1), 231–254.
Maniar, P.D., Piccoli, P.M., 1989. Tectonic discrimination of granitoids. Geol. Soc. Am. Bull. 101 (5), 635–643.
Masurel, Q., Eglinger, A., Thébaud, N., Allibone, A., André-Mayer, A.S., McFarlane, H., Miller, J., Jessell, M., Ailleres, L., Vanderhaeghe, O., Salvi, S., Baratoux, L., Perrouty, S., Begg, G., Fougerouse, D., Hayman, P., Wane, O., Tshibubudze, A., Parra-Avila, L., Kouamelan, A., Amponsah, P.O., 2022. Paleoproterozoic gold events in the Southern West African craton: review and synopsis. Miner. Deposita 57 (4), 513–537.
McFarlane, H.B., Thébaud, N., Parra-Avila, L.A., Armit, R., Spencer, C., Ganne, J., Ailleres, L., Bratoux, L., Betts, P.G., Jessell, M.W., 2019. Onset of the supercontinent cycle: evidence for multiple oceanic arc accretion events in the paleoproterozoic sefwi greenstone belt of the West african craton. Precambrian Res. 335, 105450.
Middlemost, E.A.K., 1994. Naming materials in magma/igneous rock system. earth sci. Rev. 37, 215–224.
Milési, J.P., Ledru, P., Feybesse, J.L., Dommanget, A., Marcoux, E., 1992. Early Proterozoic ore deposits and tectonics of the Birimian orogenic belt, West Africa. Precambrian Res. 58 (1–4), 305–344.
Nachit, H., Ibhi, A., Abia, E.H., Ben Ohoud, M., 2005. Discrimination entre biotites magmatiques primaires, biotites rééquilibrées et biotites néoformées. Compt. Rendus Geosci. 337 (16), 1415–1420. https://doi.org/10.1016/j.crte.2005.09.002.
Nunoo, S., Hofmann, A., Kramers, J., 2022. Geology, zircon U–Pb dating and εHf data for the Julie greenstone belt and associated rocks in NW Ghana: implications for Birimian-to-Tarkwaian correlation and crustal evolution. J. Afr. Earth Sci. 186, 104444.
Nunoo, S., Manu, J., Olarewaju, V.O., Asiedu, D.K., Nude, P.M., 2016. Deciphering structures and deformation of the obuom gold prospect, central Ashanti belt of Ghana: a lithostructural approach. J. Afr. Earth Sci. 124, 159–170.
Nunoo, S., Manu, J., Owusu-Akyaw, F.K., Nyame, F.K., 2022b. Impact of artisanal small-scale (gold and diamond) mining activities on the Offin, Oda and Pra rivers in Southern Ghana, West Africa: a scientific response to public concern. Heliyon 8 (12), e12323.
O'Connor, J.T., 1968. Mineral stability at the Martian surface. J. Geophys. Res. 73 (16), 5301–5311.
O'Connor, J.T., 1965. A classification for quartz-rich igneous rocks based on feldspar ratios. US Geol. Surv. 525B, B79–B84. *Professional Papers*.
Opare-Addo, E., Browning, P., John, B.E., 1993. Pressure-Temperature constraints on the evolution of an early Proterozoic plutonic suite in southern Ghana, West Africa. J. Afr. Earth Sci. 17 (1), 13–22.
Palme, H., O'Neill, H.S.C., 2014. Cosmochemical estimates of mantle composition. Treatise on Geochem. 2, 13.
Parra-Avila, L.A., Baratoux, L., Eglinger, A., Fiorentini, M.L., Block, S., 2019. The eburnean magmatic evolution across the baoulé-mossi domain: geodynamic implications for the West african craton. Precambrian Res. 332 (August 2018), 105392. https://doi.org/10.1016/j.precamres.2019.105392.
Pearce, J.A., 2008. Geochemical fingerprinting of oceanic basalts with applications to ophiolite classification and the search for Archean oceanic crust. Lithos 100 (1–4), 14–48. https://doi.org/10.1016/j.lithos.2007.06.016.
Peccerillo, A., Taylor, S.R., 1976. Geochemistry of Eocene calc-alkaline volcanic rocks from the Kastamonu area, northern Turkey. Contrib. Mineral. Petrol. 58 (1), 63–81.
Pearce, J.A., Harris, N.B., Tindle, A.G., 1984. Trace element discrimination diagrams for the tectonic interpretation of granitic rocks. J. Petrol. 25 (4), 956–983.
Petersson, A., Scherstén, A., Kemp, A.I., Kristinsdóttir, B., Kalvig, P., Anum, S., 2016. Zircon U–Pb–Hf evidence for subduction related crustal growth and reworking of Archaean crust within the Palaeoproterozoic Birimian terrane, West African Craton, SE Ghana. Precambr. Res. 275, 286–309.
Pitcher, W.S., 1997. The Nature and Origin of Granite. Springer Science & Business Media.
Plyusnina, L.P., 1982. Geothermometry and geobarometry of plagioclase-hornblende bearing assemblages. Contrib. Mineral. Petrol. 80 (2), 140–146.
Roberts, M.P., Clemens, J.D., 1993. Origin of high-potassium, calc-alkaline, I-type granitoids. Geology 21 (9), 825–828.
Rudnick, R.L., Fountain, D.M., 1995. Nature and composition of the continental crust: a lower crustal perspective. Rev. Geophys. 33 (3), 267–309.
Rudnick, R.L., Gao, S., 2003. Composition of the continental crust. The crust 3, 1–64.
Rudnick, R.L., Taylor, S.R., 1987. The composition and petrogenesis of the lower crust: a xenolith study. J. Geophys. Res. Solid Earth 92 (B13), 13981–14005.
Sakyi, P.A., Su, B.X., Manu, J., Kwayisi, D., Anani, C.Y., Alemayehu, M., Malaviarachchi, S.P., Nude, P.M., Su, B.C., 2020b. Origin and tectonic significance of the metavolcanic rocks and mafic enclaves from the palaeoproterozoic birimian terrane, SE West African craton, Ghana. Geol. Mag. 157 (8), 1349–1366.
Sakyi, P.A., Addae, R.A., Su, B.X., Dampare, S.B., Abitty, E., Su, B.C., Liu, B., Asiedu, D. K., 2020a. Petrology and geochemistry of TTG and K-rich paleoproterozoic birimian granitoids of the West african craton (Ghana): petrogenesis and tectonic implications. Precambrian Res. 336, 105492.
Sakyi, P.A., Manu, J., Su, B.X., Kwayisi, D., Nude, P.M., Dampare, S.B., 2019. Geochemical and Sm–Nd isotopic evidence for the composition of the palaeoproterozoic crust of the West african craton in Ghana. Geol. J. 54 (6), 3940–3957.
Sakyi, P.A., Anum, S., Su, B.X., Nude, P.M., Su, B.C., Asiedu, D.K., Nyame, F., Kwayisi, D., 2018. Geochemical and Sr-Nd isotopic records of Paleoproterozoic metavolcanics and mafic intrusive rocks from the West African Craton: evidence for petrogenesis and tectonic setting. Geol. J. 53 (2), 725–741.
Sakyi, P.A., Su, B.X., Anum, S., Kwayisi, D., Dampare, S.B., Anani, C.Y., Nude, P.M., 2014. New zircon U-Pb ages for erratic emplacement of 2213-2130Ma paleoproterozoic calc-alkaline I-type granitoid rocks in the Lawra volcanic belt of northwestern Ghana, West Africa. Precambrian Res. 254, 149–168. https://doi.org/10.1016/j.precamres.2014.08.009.
Salvi, S., Amponsah, P.O., Siebenaller, L., Béziat, D., Baratoux, L., Jessell, M., 2016. Shear-related gold mineralization in Northwest Ghana: the Julie deposit. Ore Geol. Rev. 78, 712–717.
Sapah, M.S., Agbetsoamedo, J.E., Amponsah, P.O., Dampare, S.B., Asiedu, D.K., 2021. Neodymium isotope composition of palaeoproterozoic birimian shales from the wa-lawra belt, north-west Ghana: constraints on provenance. Geol. J. 56 (4), 2072–2081.
Schmidt, M.W., 1992. Amphibole composition in tonalite as a function of pressure: an experimental calibration of the Al-in-hornblende barometer. Contrib. Mineral. Petrol. 110 (2–3), 304–310.
Senyah, G.A., Dampare, S.B., Asiedu, D.K., 2016. Geochemistry and tectonic setting of the paleoproterozoic metavolcanic rocks from the chirano gold district, sefwi belt, Ghana. J. Afr. Earth Sci. 122, 32–46.
Sepahi, A.A., Maanijou, M., Salami, S., Gardideh, S., Khaksar, T., 2012. Mineral chemistry and geothermobarometry of Moshirabad pluton, Qorveh, Kurdistan, western Iran. Isl. Arc 21 (3), 170–187.
Shabani, A.A., Lalonde, A.E., Whalen, J.B., 2003. Composition of Biotite from Granitic Rocks of the Canadian Appalachian Orogen: a Potential Tectonomagmatic Indicator? the Canadian Mineralogist.
Shand, S.J., 1943. Eruptive Rocks. Their Genesis, Composition, Classification, and Their Relations to Ore-Deposits. Wiley, New York, p. 444.
Smithies, R.H., 2000. The Archaean tonalite–trondhjemite–granodiorite (TTG) series is not an analogue of Cenozoic adakite. Earth Planet Sci. Lett. 182 (1), 115–125.
Spear, F.S., 1993. Metamorphic phase equilibria and pressure-temperature-time paths. Mineral. Soc. Am. Monograph 1, 799p.
Spencer, C.J., Roberts, N.M.W., Santosh, M., 2017. Growth, destruction, and preservation of Earth's continental crust. Earth Sci. Rev. 172, 87–106.
Stein, E., Dietl, C., 2001. Hornblende thermobarometry of granitoids from the Central Odenwald (Germany) and their implications for the geotectonic development of the Odenwald. Mineral. Petrol. 72 (1), 185–207.
Su, S., Chen, B., He, M., Hu, B., Xiao, Z., 2014. Determination of trace/ultratrace rare earth elements in environmental samples by ICP-MS after magnetic solid phase extraction with Fe3O4@ SiO2@ polyaniline–graphene oxide composite. Talanta 119, 458–466.
Sun, S.S., McDonough, W.F., 1989. Chemical and isotopic systematics of oceanic basalts: implications for mantle composition and processes. Geol. Soc. Lond. Spec. Publ. 42 (1), 313–345.
Sylvester, P.J., Attoh, K., 1992. Lithostratigraphy and composition of 2.1 Ga greenstone belts of the West African Craton and their bearing on crustal evolution and the Archean-Proterozoic boundary. J. Geol. 100 (4), 377–393.
Taylor, P.N., Moorbath, S., Leube, A., Hirdes, W., 1992. Early Proterozoic crustal evolution in the Birimian of Ghana: constraints from geochronology and isotope geochemistry. Precambrian Res. 56 (1–2), 97–111.
Tetsopgang, S., Enami, M., Njonfang, E., 2011. Emplacement P-T conditions of Pan-African biotite-amphibole granitoids in the Nkambe area, Cameroon. J. Mineral. Petrol. Sci. 106 (6), 306–319. https://doi.org/10.2465/jmps.110308.
Thieblemont, D., Tegyey, M., 1994. Geochemical discrimination of differentiated magmatic rocks attesting for the variable origin and tectonic setting of calc-alkaline magmas. Comptes Rendus De L Academie Des Sci. Serie II 319 (1), 87–94.
Thiéblemont, D., Goujou, J.C., Egal, E., Cocherie, A., Delor, C., Lafon, J.M., Fanning, C. M., 2004. Archean evolution of the Leo rise and its eburnean reworking. J. Afr. Earth Sci. 39 (3–5), 97–104.
Tshibubudze, A., Hein, K.A.A., Peters, L.F.H., Woolfe, A.J., McCuaig, T.C., 2013. Oldest U-Pb crystallisation age for the West african craton from the oudalan-gorouol belt of Burkina Faso. S. Afr. J. Geol. 116 (1), 169–181.
Uchida, E., Endo, S., Makino, M., 2007. Relationship between solidification depth of granitic rocks and formation of hydrothermal ore deposits. Resour. Geol. 57 (1), 47–56.
Wang, Z.M., Han, C.M., Xiao, W.J., Su, B.X., Sakyi, P.A., Song, D.F., Lin, L.N., 2014. The petrogenesis and tectonic implications of the granitoid gneisses from Xingxingxia in the eastern segment of Central Tianshan. J. Asian Earth Sci. 88, 277–292.
White, A.J.R., Waters, D.J., Robb, L.J., 2013. The application of P–T–X (CO 2) modelling in constraining metamorphism and hydrothermal alteration at the Damang gold deposit, G hana. J. Metamorph. Geol. 31 (9), 937–961.
Zhou, Z.X., 1986. The origin of intrusive mass in Fengshandong, Hubei province. Acta Petrol. Sin. 2 (2), 59–70.